Materials Processing Center
Prepared under Grant No. 7645

The Materials Processing Research Base of the Materials Processing Center

Annual Report for Year Ending September 30, 1986

Submitted by:

R.M. Latanision
Materials Processing Center
Massachusetts Institute of Technology
Cambridge, Massachusetts 02139

Submitted to:

National Aeronautics and Space Administration
400 Maryland Avenue S.W.
Washington, D.C. 20548

Contents

Introduction

This is the annual report of the research activities conducted at the Materials Processing Center (MPC) under the Materials Processing Research Base of NASA Grant #7645 and covers the period October 1, 1985 through September 30, 1986.

projects. In brief, these projects are:

Dielectrophoresis in the Microgravity Environment - Professor Robert M. Rose

Dielectrophoresis, the motion induced on a neutral particle by the presence of a nonuniform electric field, has, in principle, several remarkable features. Since it depends principally on the complex electrical permittivity and acceleration is independent of particle size and shape, it could be used to separate particles based on materials properties only. It is, however, a second-order effect, and the resulting forces are weak and easily wiped out by convection or turbulence. These problems are completely eliminated by the use of the microgravity/vacuum environment. To assess the use of dielectrophoresis as a materials separation technology in microgravity and/or vacuum, Professor Rose designed and constructed a free-fall, vacuum dielectrophoretic separator. The apparatus is now being used to evaluate the separation of "model" powder mixtures (ceramics, polymerics, metallics).

Phase Separation Kinetics in Immiscible Liquids - Professor Donald R. Sadoway

Miscibility gaps, both stable and metastable, exist in many technologically important systems. Control of phase separation phenomena is essential to achieve microstructures that yield desired properties in such commercially significant systems as inorganic glasses, biochemicals, semiconductors, colloidal suspensions, and high-performance metal alloys. To study the mechanisms of transformation as it occurs, Professor Sadoway used the optical imaging technique of laser schlieren to observe the resultant microstructure as it evolves in immiscible liquids, in this case, a succinonitrile-water system. Future low-gravity experiments will eliminate the stratification that occurs when the second phase particles grow beyond the size at which interfacial tension no longer counteracts the force of gravity.

Transport Properties of Droplet Clusters in Gravity-Free Fields - Professor Howard Brenner

Materials processing in a low-gravity environment could produce microstructures unobtainable in terrestrial, gravity-dominated systems. To better understand nucleation and the basic transport processes involved, specifically, the kinetics of phase transformations, Professor Brenner has begun to describe clusters of liquid droplets immersed in an atmosphere composed of the saturated vapor. By studying the rates of droplet coalescence and breakup and the coupling between such 'internal' transport processes as molecular diffusion and convection under the influence of external fields, he is modeling the system as a continuum where macroscopic properties may be determined by applying the generalized theory of Taylor dispersion.

One continuing project was funded at the seed level.

Probes and Monitors for the Study of Solidification of Molten Semiconductors - Professor Donald R. Sadoway.

Product morphology and dopant concentration in semiconductor crystal growth are strongly influenced by the behavior of the solid-liquid interface during solidification. Since in situ observation of solidification in this technologically important systems is not possible, investigators have resorted to the use of physical models, such as water and organic liquids. These models, while transparent to visible light, suffer from the fact that their Prandtl numbers are too high. Significant deviations in such properties from those of the system of interest can weaken the physical model to the extent that it does not properly reflect the real system. Molten alkali halides are better physical models in this respect and are transparent to visible light. Professor Sadoway has found that optical techniques such as laser schlieren imaging can be used to observe phenomena such as solute rejection during solidification in the LiCl-KCl system. This capability to observe melt-flow patterns and the advance of the solid-liquid interface during solidification helps to verify mathematical models and serves as the basis for control instrumentation for microgravity processing.

Finally, two independent, ongoing, major research projects were funded in this grant.

Fluid Mechanics and Mass Transfer in Melt Crystal Growth: Analysis of the Floating Zone and Vertical Bridgman Processes - Professor Robert A. Brown

The fundamental understanding of the interactions of heat and mass transport, melt flow, and the morphology of solidification interfaces is crucial to the design and interpretation of experiments on the controlled solidification of semiconductor crystal growth on earth and in space. Professor Brown has focussed this project on the finite-element analysis of the dynamics of the floating zone process for growth of small-scale crystals, the study of the effect of vertically-aligned, applied magnetic fields on convection and solute segregation in directional solidification, and the dynamics of microscopic cell formation in the two-dimensional solidification of binary alloys.

Heat Flow Control and Segregation in Directional Solidication: Development of an Experimental and Theoretical Basis for Bridgman-Type Growth Experiments in a Microgravity Environment - Professor August F. Witt

Gravitational effects are the primary cause of our inability to bridge the existing gap between theory and the practice of crystal growth. They are, therefore, the direct cause for our failure to achieve theoretical property limits in materials, the prerequisite for optimization of device performance. Previous semiconductor growth experiments in space exposed serious deficiencies in existing processing techniques. Efforts to emulate as closely as possible the conditions prevailing in the reduced gravity environments led directly to the evolution of magnetic melt stabilization and heat transfer control. Professor Witt used a superconducting magnet to generate vertical magnetic fields of up to 30 kGauss in a seeded vertical Bridgman-Stockbarger growth system. These studies demonstrate that magnetic melt stabilization can emulate a limited spectrum of reduced gravity conditions and confirms theoretical predictions of diffusion-controlled solidification. Future studies will extend the study of segregation beyond the initial transient.

5/-29

N89-13672 /175204 4P

Dielectrophoresis in the Microgravity Environment

Principal Investigator: Professor R.M. Rose

MJ 700807

Abstract

Microgravity and vacuum, singly or combined, are uniquely advantageous media for the use of dielectrophoresis as a materials separation technology. In order to assess these advantages a free-fall vacuum dielectrophoretic separator was designed and constructed for use at the earth's surface.

Introduction

"Dielectrophoresis" is the motion induced by the presence of nonuniform electric field. The field equations describing this phenomena are

$$\vec{F} = (\vec{P} \cdot \vec{\nabla})\vec{E} \tag{1}$$

$$\vec{P} = \overleftrightarrow{\alpha} \cdot \vec{E}\,v \tag{2}$$

$$\vec{F} \sim K_1 \frac{(K_2 - K_1)}{(K_2 + 2K_1)} \vec{\nabla}(E)^2 \tag{3}$$

where F is the resulting force on the particle, P the induced dipole, E the applied field, and K_1 and K_2 the relative dielectric constants of the medium and the particle, respectively. Because dielectrophoresis is so often confused with electrophoresis, Table I is presented for the reader. (This is a somewhat more elaborate presentation of an earlier comparison by Pohl.[1])

As Equation 1-3 and Table I together indicate, the dielectrophoretic effect has several remarkable features, at least in principle. The effect depends principally on the complex electrical permittivity and the acceleration is independent of particle size and shape; thus it can (at least potentially) be used for separations based on materials properties only, as in the classical mineral separation technologies based on density which are used at the earth's surface. The principal disadvantage is that it is a second-order effect and the resulting forces are weak unless high fields (and gradients) are used. At the earth's surface, particularly when a suspending medium is used, the fields will be limited by the properties of the medium and convection will usually wipe out the effect or at least render the separation irreproducible, difficult or both. These problems are completely eliminated by use of the microgravity/vacuum environment. The remaining problem is the presence of relatively strong, first-order forces due to residual static electrical charge on the particles to be separated. This problem is effectively dealt with by utilization of the effect implied by Eq. (3), that is, that the effect is independent of the sign of the applied field; the dielectrophoretic force always has the sense of the more intense field, regardless of field direction. Thus, alternating fields, in which the forces due to direct

Table I. A Comparison of Electrophoresis with Dielectrophoresis

	Electrophoresis	Dielectrophoresis
Induced Force and Velocity:	Depends on sign of charge and sign of field. Field reversal reverses motion. Force depends on charge; does not depend directly on volume.	Independent of sign of applied field. Particle moves to more intense field. Force is proportional to volume of particle.
Induced Acceleration:	Acceleration α $1/r^2$ Excellent at molecular level.	Acceleration independent of size or shape. Feeble at molecular level unless large gradients are used.
Field Requirements:	Homogeneous or inhomogeneous fields.	Inhomogeneous fields only. Usually requires strong field gradients to overcome convection, diffusion.
	High (eg., 1 kV/m) fields, typically.	High to very high, typically 1-10 kV/m.
	Steady (DC) fields only.	Steady (DC) or alternating fields.

effects are oscillatory, do not affect the direction of the dielectrophoretic force at all. In an operating separation system the direct forces would be dealt with by the use of AC fields, and the primary technical problem in this connection would be to insure that the amplitude of oscillation induced by direct forces would be reasonable compared to the dimensions of the system. For some classes of materials the effect may be optimized by using the frequency dependence of the dielectric constants.

Additionally, because recent advances have occurred in the understanding of gravitationally-driven and capillarity-driven (i.e., Marangoni-Levich) convection, the prospect for substantial progress in separation technology as the earth's surface may exist as well. To begin with a test was desired of the feasibility of vacuum/microgravity separations by dielectrophoresis. The instrumentality elected was free-fall separation in vacuum.

Design Considerations

In order to achieve maximum separation with simple electrode geometry, coaxial cylinders were decided on, at the expense of uniformity of acceleration. (Later modification to isomotive electrode geometry was allowed for.) A preliminary assessment of lateral oscillatory amplitude at audio frequencies indicated that a system width in the range 1 – 10 cm would probably suffice; in any case, the amplitude could be decreased by increasing particle size and thereby decreasing the charge/mass ratio, assuming static charging. The amplitude would of course depend on the frequency, which was limited by practical considerations to the audio range, i.e., 20 Hz – 20 KHz. At such frequencies voltages on the order of 10 KV may be attained by pushing the state of the art of transformer design, which we did. For concentric cylindrical electrodes with 150 mm and 3 mm diameters, lateral accelerations were calculated to be in the 0.001 – 0.01 g range, depending on dielectric properties. A six-foot free-fall (dictated mainly by ceiling height in our laboratory) would then result in lateral displacements of at least a few mm, easily observable. Even small differences in dielectric properties should then result in particulate segregations which are observable at low magnification and analyzable by, e.g., the EDXA method.

ORIGINAL PAGE IS
OF POOR QUALITY

Construction of the Free-Fall Separator

The final form of the device is shown in Figures 1 and 2. The outer electrode is an evaporated

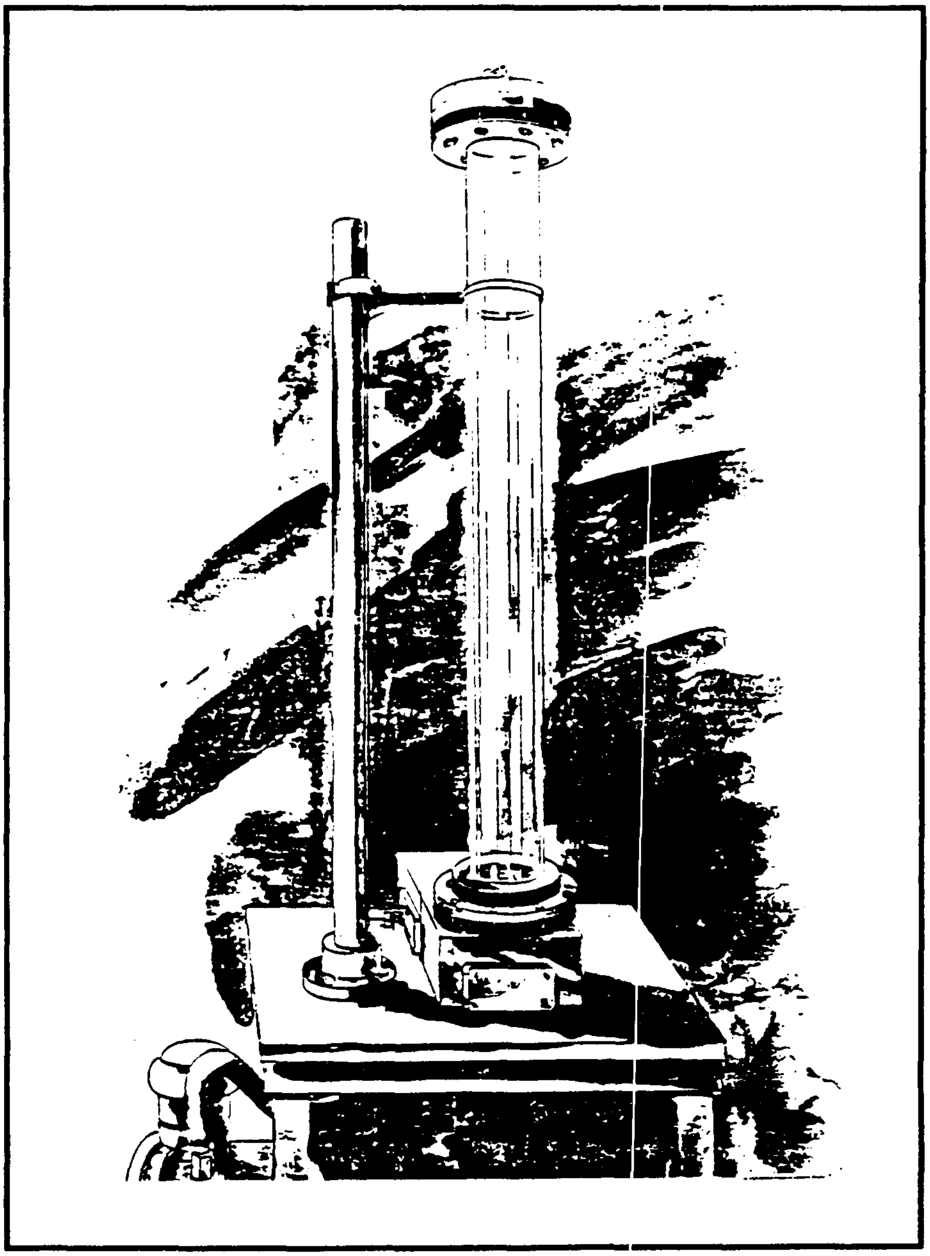

Figure 1. Free-fall Separator.

gold film deposited on the interior of the Pyrex tube; the inner electrode is polished stainless steel. At the top is a concentric mechanical iris, motor-driven for the sake of safety and to avoid vibration of the column. At the bottom is a platform supported by a removable access plate. Mixed powders will be dropped through the iris and collected on adhesive-coated slides or even small containers for examination. Below the platform and access plate is the vacuum plenum. The system is pumped through this plenum by a water-cooled, two-inch diffusion pump backed by a 5 cfm mechanical pump. Vacuum instrumentation consists of a Bayard-Alpert ionization gauge and a thermocouple gauge. The system has been pumped out and is usually kept under vacuum. The ultimate vacuum is slightly above 10^{-8} torr.

ORIGINAL PAGE IS
OF POOR QUALITY

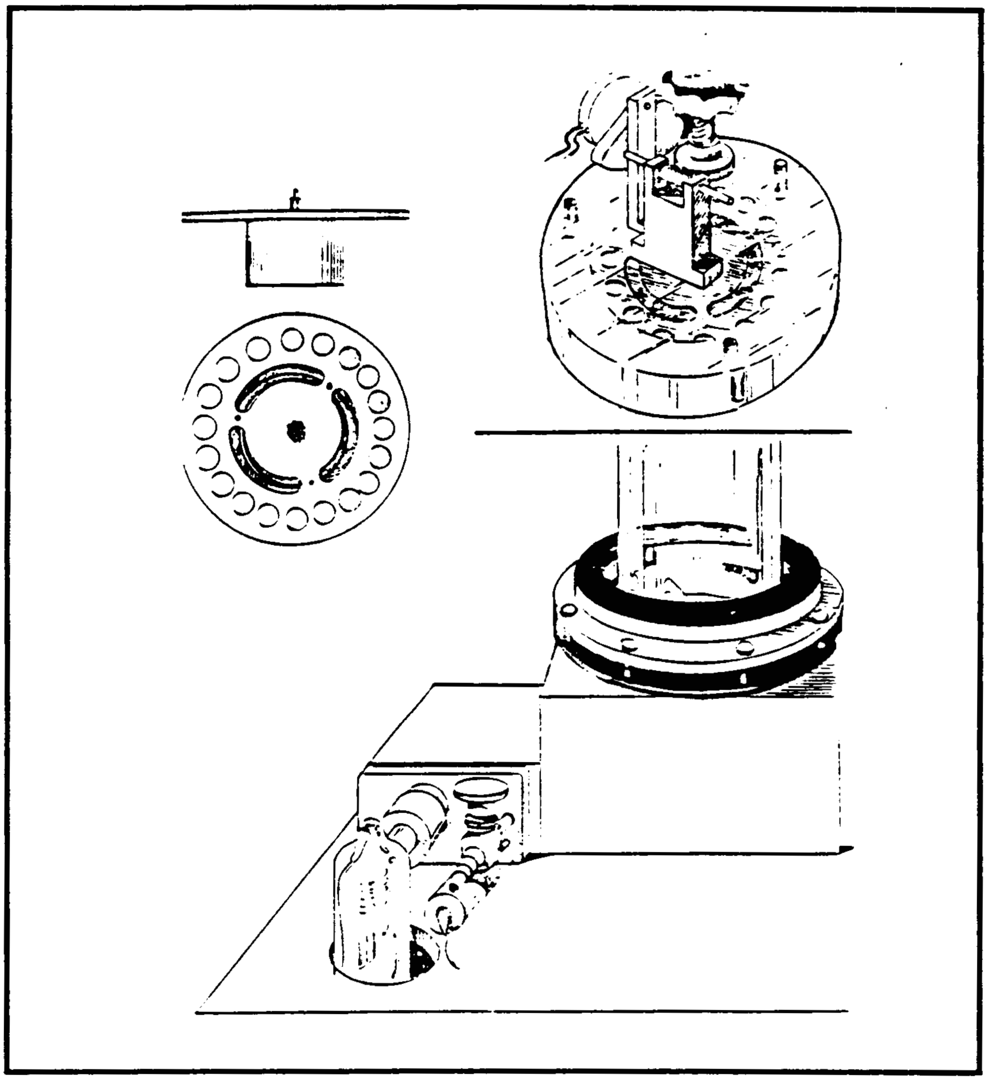

Figure 2. Detail of the Free-fall Separator.

The system is designed to be driven at 20 Hz – 20KHz at voltages up to 10 KV (RMS) by a 250 watt audio amplifier coupled to the electrodes by a transformer. Performance at the high-frequency end of this range will be limited by the capacitance of the separator (about 26 pF); the characteristics of the transformer, including the capacitance and inductance of the secondary; and, related to these concerns, by nearby resonances. Considerable difficulty was encountered obtaining adequate designs and hardware for this purpose, which we now have from two sources. At this time we do not expect to be able to drive this system to 10 KV at the highest frequencies, but in general, the performance should be more than adequate for our experimental objectives.

Utilization

The system is now ready for use. The general scheme is to evaluate the separation of "model" powder mixtures (ceramics, polymerics, metallics) and develop quantitative models applicable to microgravity conditions. Some analysis of dynamic effects, particularly those resulting from relaxations, will be attempted.

Reference List

1. H.A. Pohl, "Dielectrophoresis," (Cambridge University Press, 1978).

N89 - 13673

S3-25
175305
3P

Phase Separation Kinetics in Immiscible Liquids

Principal Investigator: Professor D.R. Sadoway

MJ 700202

Abstract

The kinetics of phase separation in the succinonitrile-water system are being investigated. Experiments involve initial physical mixing of the two immiscible liquids at a temperature above the consolute, decreasing the temperature into the miscibility gap, followed by imaging of the resultant microstructure as it evolves with time Refractive index differences allow documentation of the changing microstructures by noninvasive optical techniques without the need to quench the liquid structures for analysis.

Introduction

Miscibility gaps, both stable and metastable, are known to exist in many technologically important systems. Control of phase separation phenomena is essential in achieving microstructures that yield desired properties. In this regard it is imperative that the transformation kinetics be well understood.

In many cases heterogeneous interconnected microstructures result. In early studies investigators were prompted to conclude that the mechanism of transformation is spinodal decomposition.[1] Further work has cast doubt upon some of the conclusions of these investigations and indicated that inference of the mechanism of separation from observations of the final phase morphologies can be completely misleading.[2-7] It is clear that the kinetics of the transformation must be studied as it occurs, especially during its earliest stages when differences in mechanism are best elucidated. The later stages of any transformation are dominated by coarsening kinetics.[2-8]

Reduced gravity offers the opportunity to produce microstructures unattainable on earth. Specifically, it is possible to solidify two-phase liquids as dispersions, thereby yielding exciting properties as a consequence of the metastable microstructure. The generation of dispersed second phase droplets in reduced gravity poses interesting questions in phase transformation kinetics. It is well known from the now classical studies of solid-solid transformations that within the miscibility gap phase transformation occurs not simply by nucleation and growth but, over well defined regions of composition and temperature, by spinodal decomposition instead. The same behavior is expected with liquid-liquid phase transformations. From the standpoint of fundamental studies liquid-liquid phase transformations are interesting because "matrix effects" present during the demixing of solid solutions are not expected to be significant in liquids.

The Present Study

The present study is an attempt to follow phase separation kinetics in immiscible liquids. The classical studies separation have been done on solid phase system: liquids stratify in a gravity field. Thus, the two principal techniques are electron microscopy and electromagnetic scattering (both light scattering and small angle x-ray). In low-gravity phase separation studies of liquids that are transparent to visible light a variety of optical imaging techniques based upon differences in refractive index become available, for example, laser schlieren imaging.[9] Experiments then involve an initial physical mixing of the two immiscible liquids followed by imaging of the resultant microstructure as it evolves with time.

Reduced gravity studies are important because they allow the observation of phase separation without stratification which occurs when the second phase particles grow beyond the size at which interfacial tension no longer counteracts the force of gravity. In reduced gravity there is no need to alter the relative densities or interfacial energies of the two phases by adding stabilizers, nor is it necessary to quench the liquid structures for analysis. Furthermore, the experiments can be repeated by simply remixing. As part of the present study, laboratory scale equipment is being designed and built such that it can be readily adapted for zero gravity flight.

The results will be compared with theory. For constant volume fractions of the separated phases, the average particle diameter is expected to increase as the cube root of time and the number of particles to decrease as the reciprocal of time.[10] Much work has been done in oxide glass systems and has been exhaustively reviewed by Uhlmann and Kolbeck.[11] While agreement is good for systems undergoing spinodal decomposition, there is no comprehensive analysis for phase separation by the competing nucleation and growth mechanism

It has been suggested that electron microscopy be used to differentiate between nucleation and growth and spinodal decomposition.[12] For nucleation and growth the volume fraction transformed should increase with time (following an incubation period), while for spinodal decomposition the volume fraction should in many cases decrease with time to reflect a transition from compositional waves symmetric about the mean concentration to compositional waves fluctuating between the equilibrium concentrations (seen as relative volume fraction) of the two phases. The experimental technique should be able to observe the decrease in second-phase volume fraction during the period of this transition. Such measurements, however, are not simple because of the difficulties in differentiation between the two phases and in accurately determining their volume fractions. One of the goals of the initial phase of this study is to develop the optical techniques to permit such accurate measurements.

The physical system under investigation is succinonitrile-water which exhibits liquid imiscibility and has a consolute temperature of 56°C.[13] However, the compositional dependence of several important physical properties is not know, specifically, the density and interfacial tension. As a result, density measurements by the direct Archimedean technique are being performed to support the kinetic studies described above.

The results of this study will be of importance in commercially significant systems such as inorganic glasses, biochemicals, semiconductors, colloidal suspensions, and aircraft metal alloys.

Reference List

1. J.W. Cahn and R.J. Charles, *Physics Chem. Glasses* 6 (1965): 181.

2. W. Haller, *J. Chem. Phys.* 42 (1965): 686.

3. R.W. Hopper and D.R. Uhlmann, *Disc. Faraday Soc.* 56 (1970): 166.

4. G.R. Srinivasan, J. Tweer, P.B. Macedo, A. Sarker, and W. Haller, *J. Non-cryst. Solids* 6 (1971): 221.

5. T.P. Seward III, D.R. Uhlmann, and D. Turnbull, *J. Am. Ceram. Soc.* 51 (1968): 634.

6. W. Haller and P.B. Macedo, *Physics Chem. Glasses* 9 (1968): 153.

7. P.F. James and P.W. McMillan, *Physics Chem. Glasses* 11 (1970): 59 and 11 (1970): 64.

8. J. Zarzycki and F. Naudin, *J. Non-cryst. Solids* 1 (1969): 215.

9. J.K. Koziol and D.R. Sadoway, "Electrolyte Flow Patterns in Molten Salt Electrolysis Cells," *Energy Reduction Techniques in Metal Electrochemical Processes*, eds. R.G. Bautista and R. Wesely (Warrendale, PA:TMS-AIME, 1985).

10. D.G. Burnett and R.W. Douglas, *Physics Chem. Glasses* 11 (1970): 125.

11. D.R. Uhlmann and A. G. Kolbeck, *Physics Chem. Glasses* 17 (1976): 146.

12. G.R. Srinivasa, A. Sarkar, P.K. Gupta, and P.B. Macedo, *J. Non-cryst. Solids* 20 (1976): 141.

13. J.E. Smith, Jr., D.O. Frazier, and W.F. Kaukler, *Scripta Met.* 18 (1984): 677.

N89-13674 S3-29 / 158065 6P.

Transport Properties of Droplet Clusters in Gravity-Free Fields

Principal Investigator: Howard Brenner

Abstract

Clusters of liquid droplets are suspended in an atmosphere of saturated vapor and are subjected to an external force field. This system can be modeled as a continuum whose macroscopic properties may be determined by applying the generalized theory of Taylor dispersion.

Background

In many recent studies[1-4] the phenomenological theory of nucleation[5] has been derived starting from the more fundamental description of critical phenomena.[6] In most applications, however, a coarser grained description of the system is required, where the two-phase medium is modeled as a continuum whose macroscopic properties depend on the fine-grained geometric characteristics of the system and on the physical properties of the two phases. In the research program that we have undertaken this goal is pursued for the particular case of liquid droplets immersed in an atmosphere composed of its saturated vapor. This study requires a fundamental understanding of the basic transport processes involved -- specifically, knowledge of the kinetics of phase transformation (involving, for example, rates of droplet coalescence and breakup) and the coupling between such 'internal' transport processes, typically molecular diffusion and convection under the influence of external fields. We expect that the dominance of capillary forces in our two-phase, gravity-free systems will lead to novel physicochemical two-phase interfacial phenomena, not encountered in terrestrial, gravity-dominated systems.

Our approach to the problem uses the following scheme:

a) Formulate the problem at a microscale level such that the droplets are perceived as discrete entities[5] and where interfacial effects can be taken into consideration using macroscopic relations.[7-13]

b) Apply the generalized theory of Taylor dispersion [14-16] to the problem to obtain a set of model equations (presumably of the convective-diffusive type), describing the system as a continuum at the macroscale.

Results

Our analysis applies to spherical liquid droplets (or vapor bubbles) of radius r at position R = (s, y, z) in a vapor (or liquid) continuum, with σ_0 the surface tension. It begins with the observation that at thermodynamic equilibrium (and in the absence of a gravity field causing sedimentation of the

PRECEDING PAGE BLANK NOT FILMED

PAGE 12 INTENTIONALLY BLANK

denser phase) the probability density $P_0^\infty(r)$ for finding droplets of size r at any point R of space is independent of R, and is given by[5]

$$P_0^\infty(r) = C^{\left\{\frac{4\pi\sigma_0}{3kT} r^2\right\}}, \tag{1}$$

with kT the Boltzmann factor and C the normalization constant

$$C = 32\pi\,(\sigma_0/3kt)^{3/2} \tag{2}$$

arising from the unit normalization condition

$$\int_0^\infty P_0^\infty(r) r^2 dr = 1 \tag{3}$$

impose on the probability.

One of our main accomplishments to date is the derivation[17] of the kinetic equation

$$\frac{\delta P}{\delta t} + \nabla \cdot\ J = \frac{1}{r^2}(r^2 j) = 0 \tag{4}$$

governing the **nonequilibrium** transport of the probability density

$$P = P(r,R,t), \tag{5}$$

$$\int_{R=0}^\infty d^3R \int_{r=0}^\infty P\, r^2 dr = 1, \tag{6}$$

for finding droplets of size r at position R. In the preceding,

$$\nabla \equiv (\delta/\delta R)_r = i(\delta/\delta x) + j(\delta/\delta y) + k(\delta/\delta x) \tag{7}$$

is the R-space gradient operator, and

$$d^3R - dx\,dy\,dz \tag{8}$$

is a physical-space volume element. Here, the convective-diffusive constitutive equation for the fluxes appearing in the conservation equation (4) are, respectively,

(i) size-space flux density:

$$j = uP - d(r)\frac{\delta P}{\delta r}; \tag{9}$$

(ii) physical-space flux density vector:

$$J = U(r)P - D(r)\nabla P. \tag{10}$$

Phenomenological coefficients appearing in the above are with μ_0 the viscosity of the continuous phase,

$$u = -\frac{\sigma_0}{6\mu_0}, \tag{9a}$$

$$d(r) = \frac{kT}{16\pi\mu_0 r} \tag{9b}$$

and

$$U(r) = M(r)F, \tag{10a}$$

$$D(r) = kTM(r), \tag{10b}$$

with

$$M(r) = (6\pi\mu_0 r)^{-1} \tag{10c}$$

the Stokes law mobility of the droplet. In addition, F is the external force, if any, exerted on the droplet.

The zeroth-order moment

$$P_0 \overset{def.}{=} \int_{R=0}^{\infty} d^3R\, P \tag{11}$$

of the probability density P satisfying the kinetic equation (4)-(10) properly reduces in the steady state, $t \to \infty$, to the original equilibrium relation (1). On the other hand, if the system is not at equilibrium [e.g. all the droplets are initially of identical size, rather than conforming to the equilibrium size distribution (1)], Eqs. (4)-(10) permit calculation of the detailed relaxation of the droplet size distribution of the system to its equilibrium state (1). Simultaneously, it also allows calculation of the relaxation of **spatial** gradients existing within the system. In particular, it reveals how these two transport processes are coupled.

Equations (4)-(10) are identical in structure to the generic equations of generalized Taylor dispersion theory,[14-15] thus permitting determination of the macroscopic properties of the two-phase system. For example, we find that the sized-averaged molecular diffusivity,

$$\bar{D}_M \overset{def.}{=} \int_0^{\infty} P_0^{\infty}(r) D(r) r^2 dr, \tag{12}$$

of the system is

$$\bar{D}_M = \frac{2(kT\sigma_0)^{1/2}}{3\sqrt{3}\pi\mu_0}. \tag{13}$$

Moreover, if a force f per unit volume is applied to the discrete phase (i.e. $f = F/(4\pi r^3/3)$, the total diffusivity coefficient $\bar{D}^*$ adopts the form

$$\bar{D}^* = \bar{D}_M + \bar{D}_C\,, \tag{14}$$

with $\bar{D}_C$ denoting the Taylor-like convective contribution

$$\bar{D}_C = \frac{7}{486\pi^3}\left\{\frac{3kT}{\sigma_0}\right\}^{5/2} \frac{f^2}{\sigma_0\mu_0} \tag{15}$$

to the diffusion coefficient. It is generally only these **mean** types of phenomenological quantities that are directly accessible to experiments, rather than comparable size-specific phenomenological coefficients, such as D and d appearing in Eqs. (9) and (10). Closely related to this is the fact that Eqs. (13) and (15) involve only macroscopic physical parameters, namely interfacial tension σ_0 and continuous-phase viscosity μ_0.

Extensions of the Research

Fundamental solution of the kinetic equation. We are currently attempting to provide the fundamental Green's function solution of the unsteady kinetic equation. by the method of superposition this will reduce the solution of the kinetic equations for an arbitrary initial size distribution to a quadrature. The existence of such formal solutions will prove useful in future applications by permitting calculation of the relaxation of the system to its equilibrium state.

Finite container size. As in Eq. (3), droplet radii in the range $r = 0$ to ∞ are employed in the development Obviously, finite container dimensions preclude from consideration relatively large droplet sizes. Thus, in applying our equations in practice, attention needs to be paid to rationally deriving an upper cutoff radius r_0 in relation to the container size.

Lower limit cutoff radius. If the droplets are too small, our kinetic analysis may become inapplicable, owing to the breakdown of the continuum hypothesis. Whether or not such effects are significant remains to be examined.

N particle approach. Hydrodynamic interaction between Brownian droplets. Our ideal kinetic equations effectively represent a one-body particle distribution P. In order to enhance the range of applicability of our analysis we need to create a more general N-body kinetic scheme, in which the (average) number of droplets is not conserved in a nonequilibrium system owing to droplet coalescence and breakup processes. One eventual prediction of our theory should be the **number of droplets** (irrespective of size r) per unit volume at a point R of the continuum, which may prove to be an experimentally accessible quantity. This requires a basic extension of the theory. Among other things, it entails problems of clustering in relation to hydrodynamic interactions among the droplets.

Surfactants. The presence of surface active agents in experimental systems is largely unavoidable. Conversely, the addition of surfactants to two-phase systems often leads to interesting new capillary phenomena, e.g. ultralow tension systems. We intend to investigate the modifications in our theory engendered by the presence of such agents. At a minimum, their presence in the form of an absorbed interfacial phase lowers the surface tension in accordance with Gibb's formula

$$\sigma = \sigma_0 - kT\Gamma_s, \tag{16}$$

where Γ_s is the surface-excess surfactant concentration at the interface. For a fixed mass of surfactant present in the system (assumed to be entirely absorbed at the interface for all times), this has the effect of making δ in Eq. (16) a function of r. As our kinetic theory has involved the assumption that $\sigma \neq \sigma(r)$, necessary modifications of the theory arising from the presence of surfactants will need to be addressed in order to gauge their experimental importance.

Supersaturated systems. Our kinetic approach may provide alternative insights into the standard approaches to the kinetics of phase transitions.[18] Such possibilities will be investigated.

Reference List

1. J.S. Langer, "Kinetics of metastable states," *Systems Far From Equilibrium*, ed. L. Garrido (Berlin:Springer, 1980), pp. 12-47.

2. K. Binder, "Spinodal decomposition," *Systems Far From Equilibrium*, ed L. Garrido (Berlin:Springer, 1989), pp. 76-90.

3. K. Kavasaki and T. Ohta, "Kinetics of fluctuations for systems undergoing phase transitions - Interfacial approach," *Physica* 118A (1983): 175-190.

4. I. Edrei and M. Gitterman, "Transient effects in nucleation for two-dimensional system," *J. Chem. Phys.* 85 (1986): 190-198.

5. *Nucleation*, ed. A.C. Zettlemoyer (New York:Marcel Dekker, 1969).

6. S. Ma, *Modern Theory of Critical Phenomena* (Reading, MA:Benjamin, 1976).

7. H. Brenner, "A micromechanical derivation of the differential equation of interfacial statics," *J. Colloid Interface Sci.* 68 (1979): 422-439.

8. H. Brenner and L.G. Leal, "Interfacial resistance to interphase mass transfer in quiescent two-phase systems," *AIChE J.* 24 (1978): 246-254.

9. H. Brenner and L.G. Leal, "A micromechanical derivation of Fick's law for interfacial diffusion of surfactant molecules," *J. Colloid Interface Sci.* 65 (1978): 191-209.

10. H. Brenner and L.G. Leal, "Conservation and constitutive equations for adsorbed species undergoing surface diffusion and convection at a fluid-fluid interface," *J. Colloid Interface Sci.* 88 (1982): 136-184.

11. S.P. Lin and H. Brenner, "Marangoni convection in a tear film," *J. Colloid Interface Sci.* 85 (1982): 59-65.

12. S.P. Lin and H. Brenner, "Tear film rupture," *J. Colloid Interface Sci.* 89 (1982): 226-231.

13. M. Vignes-Adler and H. Brenner, "A micromechanical derivation of the differential equation of interfacial statics. III. Line tension," *J. Colloid Interface Sci.* 103 (1985): 11-44.

14. H. Brenner, "A general theory theory of Taylor dispersion phenomena," *PhysicoChem. Hydrodyn.* 1 (1980): 91-123.

15. H. Brenner, "A general theory of Taylor dispersion phenomena. II. An extension," *PhysicoChem. Hydrodyn.* 3 (1982): 139-157.

16. H. Brenner, A. Nadim, and S. Haber, "Long-time molecular diffusion, sedimentation and Taylor dispersion of a fluctuating cluster of interacting Brownian particles," *J. Fluid Mech.* (in press, 1986).

17. H. Brenner and R. Mauri, "Size dispersion phenomena in two-phase systems," *J. Colloid Interface Sci.* (in preparation, 1986).

18. J. Heicklen, *Colloid Formation and Growth: A Chemical Kinetics Approach* (New York:Academic, 1976).

List of Publication Support by NSG-7645

1. A. Nadim, "Transport and statistical mechanics of flexible chains and clusters of Brownian particles in quiescent viscous fluids, Ph.D. dissertation, MIT, Cambridge, MA (May 2, 1986), 158pp.
2. H. Brenner, A. Nadim, and S. Haber, "Sedimentation and dispersion of flexible chains and clusters of hydrodynamically-interacting Brownian particles," *Proceedings of the SIAM Conference on Multiphase Systems*, ed. G. Papanicolau (Philadelphia:SIAM, in press) :21 pp.

3. H. Brenner, A. Nadim, and S. Haber, "Long-time molecular diffusion, sedimentation and Taylor dispersion of a fluctuating cluster of interacting Brownian particles," *J. Fluid Mech.* (submitted, 1986): 93.

4. H. Brenner and R. Mauri, "Size-dispersion phenomena in two-phase systems, *J. Colloid Interface Sci.* (in preparation, 1986).

5. H. Brenner, L. Ting, and D.T. Wasan, "Surface-Excess Interfacial Conservation Laws and Constitutive Equations: A Rational derivation Via Matched Asymptotic Expansions," *Physicochem. Hydrodyn.: Interfacial Phenomena*, Vol. 1, NATO ASI & EPS Conference Proceedings, Huelva, Spain, ed. M. Verlarde (New York:Plenum, in preparation, 1986).

N89 - 13675

S4-76
175207
7P

MJ 710800

Probes and Monitors for the Study of Solidification of Molten Semiconductors

Principal Investigator: Professor D.R. Sadoway

Abstract

Product morphology in metal casting and semiconductor crystal growth is strongly influenced by the nature of the solid-liquid interface during solidification. Since *in situ* observation of solidification in these technologically important systems is not possible, investigators have resorted to the use of physical models, such as water and organic liquids, which while they are transparent to visible light, suffer from the fact that their Prandtl numbers are too high. Molten alkali halides are better physical models in this respect, and are transparent to visible light. The purpose of the present study is to examine solidification in the LiCl-KCl system to determine if phenomena such as solute rejection can be observed by laser schlieren imaging.

Introduction

The properties and performance of a material are determined by its structure and composition, both of which are to a large extent controlled through processing. In semiconductor crystal growth, for example, product morphology and dopant concentration are strongly influenced by the behavior of the solid-liquid interface during solidification, yet it is difficult to observe directly. Accordingly, it is necessary to resort to mathematical models and physical models must be chosen with a high degree of similarity to the system of interest, i.e., Prandtl number, Jackson α factor, etc. Significant deviations in such properties from those of the system of interest can weaken the physical model to the extent that it cannot be assumed that certain phenomena observed in the model occur at all in the real system. This is particularly true for nontrivial solidification processes, such as solute redistribution in a multicomponent system. As another example, the problem of dendrite growth in metals has long been the subject of study. Many theories have been enunciated [1, 2, 3,]; however, it is extremely difficult to test them. Since *in situ* observation of solidification in molten metals is not possible, investigators have used physical models such as water and organic liquids, which are transparent to visible light. Table I compares the physical properties of several melts of technological significance to those of various analogs. Metals and elemental semiconductors have low Prandtl numbers ($Pr < 10^{-2}$), while water and organic liquids have high Prandtl numbers ($Pr > 10$). In the solidification of elemental semiconductors, the Jackson α factor (approximated here as $\Delta H_{fusion}/RT_{melting}$ and designated μ) is greater than 2, while in the solidification of many organic liquids $\mu < 2$. Such disparities in the Prandtl number and μ are unacceptable for the reasons given above.

With these considerations in mind, the present study has turned to the use of molten alkali chlorides as physical models representative of systems of commercial interest.

Table 1. Physical Properties of Selected Liquids

Property	Cu	Si	H_2O	SCN	KCl-LiCl
molecular weight (g mol^{-1})	63.55	28.09	18	80.09	55.47
melting temp, T_{mp} (°C)	1083	1412	0	58.08	355
heat of fusion, ΔH_f (J mol^{-1})	13,050	50,550	6008	3700	13,083
$\mu = \frac{\Delta H_f}{RT_{mp}}$	1.18	3.58	2.65	1.41	2.71-3.06
viscosity, η (Pa·s) x 10^3	4.0	1	1.787	4.6	1.46
thermal conductivity, κ_{th} ($Wm^{-1}K^{-1}$)	165.6	31	0.561	0.223	0.6903
density, ρ (kg m^{-3})	8000	2520	1000	970	1577
heat capacity, C_p (J $mol^{-1}K^{-1}$)	31.46	26.12	75.91	160	72.31
Prandtl Number *	1.2×10^{-2}	3×10^{-2}	> 13	41	< 6
crystal structure	fcc	diamond	hexagonal	bcc	sc

* computed at T_{mp}.

The Present Study

As part of an investigation of the use of molten salts as physical models in solidification processes, fluid flow patterns in the melt are being studied by laser schlieren imaging.

Figure 1 is a schematic of the experimental apparatus. The salt melt is contained in a fused quartz cell which has a square cross-section, 2" on edge. The cell is set inside an electrical resistance furnace with two viewing ports. A water cooled copper chill makes contact with the cell wall along one side. Schlieren imaging is accomplished through the use of a 5 mW helium-neon laser. The initial 0.8 mm diameter beam is expanded to 22 mm diameter before entering the cell. A lens focuses the light leaving the cell. At the focal point there is a removable knife edge mounted on an x-y-z translator. A 35 mm camera body is positioned so that its film plane coincides with the image plane of the cell. Finally, a thin, straight wire is interposed between the laser source and the cell to act as a reference against which differences in index of refraction can be viewed.

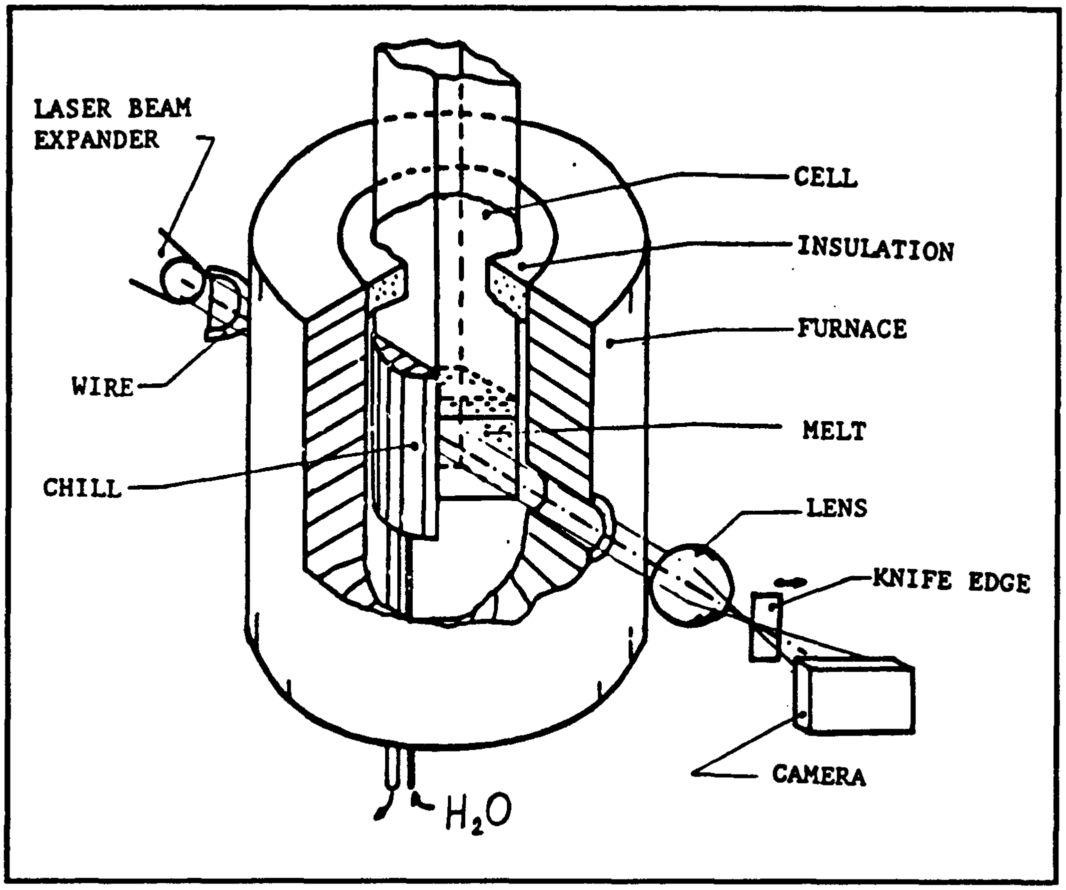

Figure 1. Schematic drawing of the experimental set-up.

In a typical experiment the purified salts are charged and melted in the cell. Then cooling water is fed to the chill and the resulting convection patterns are observed.

Two melt compositions have been chosen both in the LiCl-KCl system: the eutectic (41.5 mole% KCl) and an off-eutectic solution (46.2 mole% KCl).

Figure 2 shows a laser shadowgraph image of solidification of the eutectic melt. In a shadowgraph the schlieren knife edge has been removed from the light path. The chill plate is to the right of the field of view. Growth of solid phase is occurring in two directions: top down and bottom up. Dendrites near the cell wall are faceted; interior dendrites are not. Instead, they are thinner with multiple branches which sometimes broke off and fell (see Fig. 2(a). Weak convective motion could be detected by schlieren imaging as seen in Figure 3.

Figures 4 and 5 show images selected during the solidification of the off-eutectic melt. The process was different in this example. First, there was only one growth direction, horizontally outward from the chill. Secondly, turbulent convection was observed. The general behavior of the schlieren images can be characterized as horizontal, wavelike motion at a frequency of ~ 0.5 Hz. The source of these oscillations is presumed to be double diffusive instability. Since denser KCl is crystallizing the colder liquid close to the solid-liquid interface is richer in the less dense LiCl. Initially, the temperature effect on density dominates and the melt sinks. However, it appears that heat transfer is more rapid than mass transfer: the melt temperature rises and the compositional

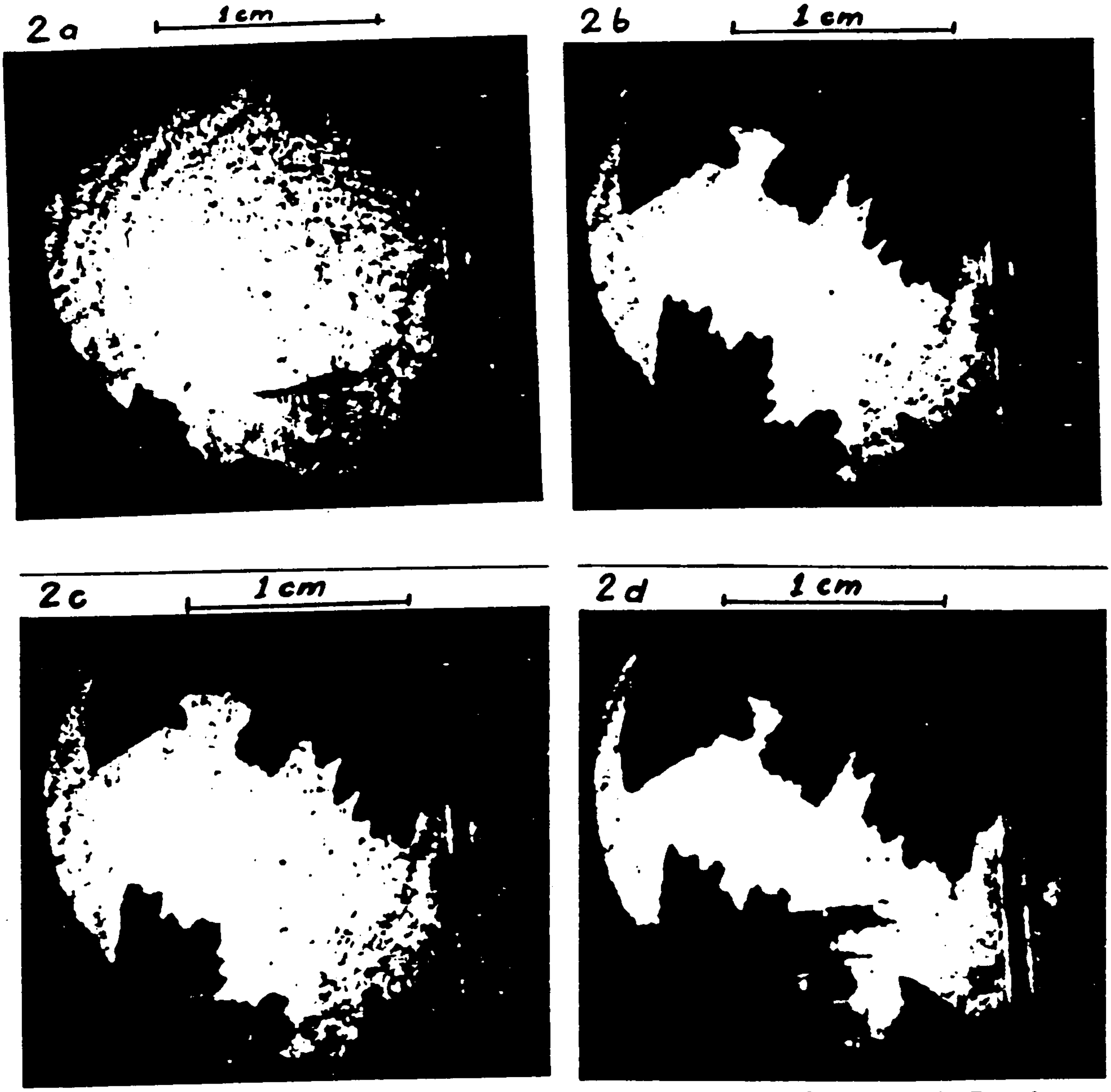

Figure 2. Shadowgraphs of solidifying KCl-LiCl eutectic melt. Chill placed beyond field of view to the right. Time of photograph reported in minutes from beginning of experiment: (a) 23, (b) 24.17, (c) 25.75, and (d) 28.67.

effect begins to dominate. This is evident in the "plumes" of the schlieren and shadowgraph images in Figure 5.

Conclusions

Molten salts have attributes that make them attractive as physical models in solidification studies. With optical techniques of investigation such as schlieren imaging it is possible to study fluid flow phenomena in molten salts and to watch the trajectory of the solid-liquid interface. Experiments are continuing.

ORIGINAL PAGE IS
OF POOR QUALITY

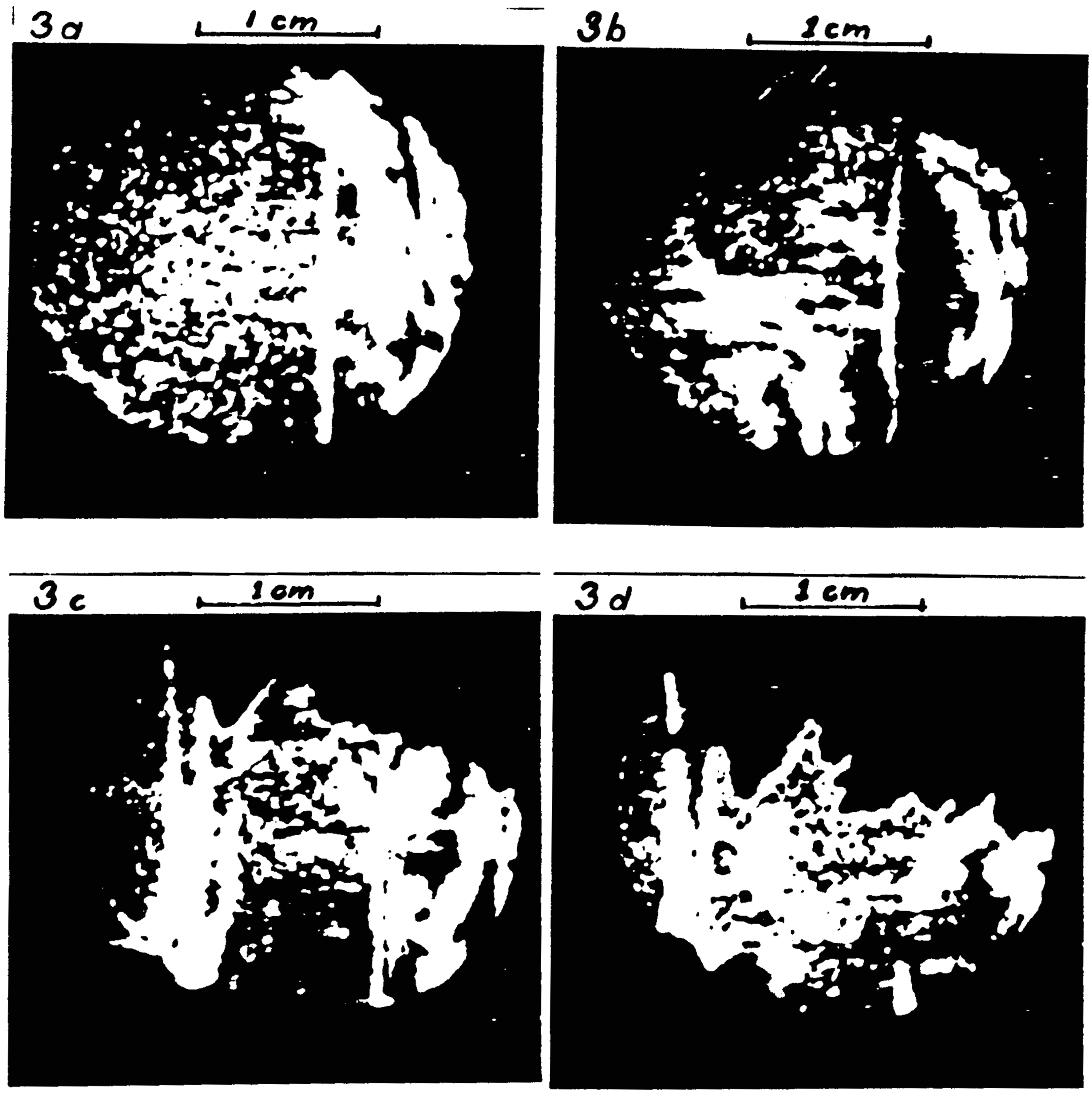

Figure 3. Schlieren images of solidifying eutectic melt. Chill placed beyond field of view to the right. Time of photograph reported in minutes from beginning of experiment: (a) 6, (b) 17.5, (c) 20.33, and (d) 24.5.

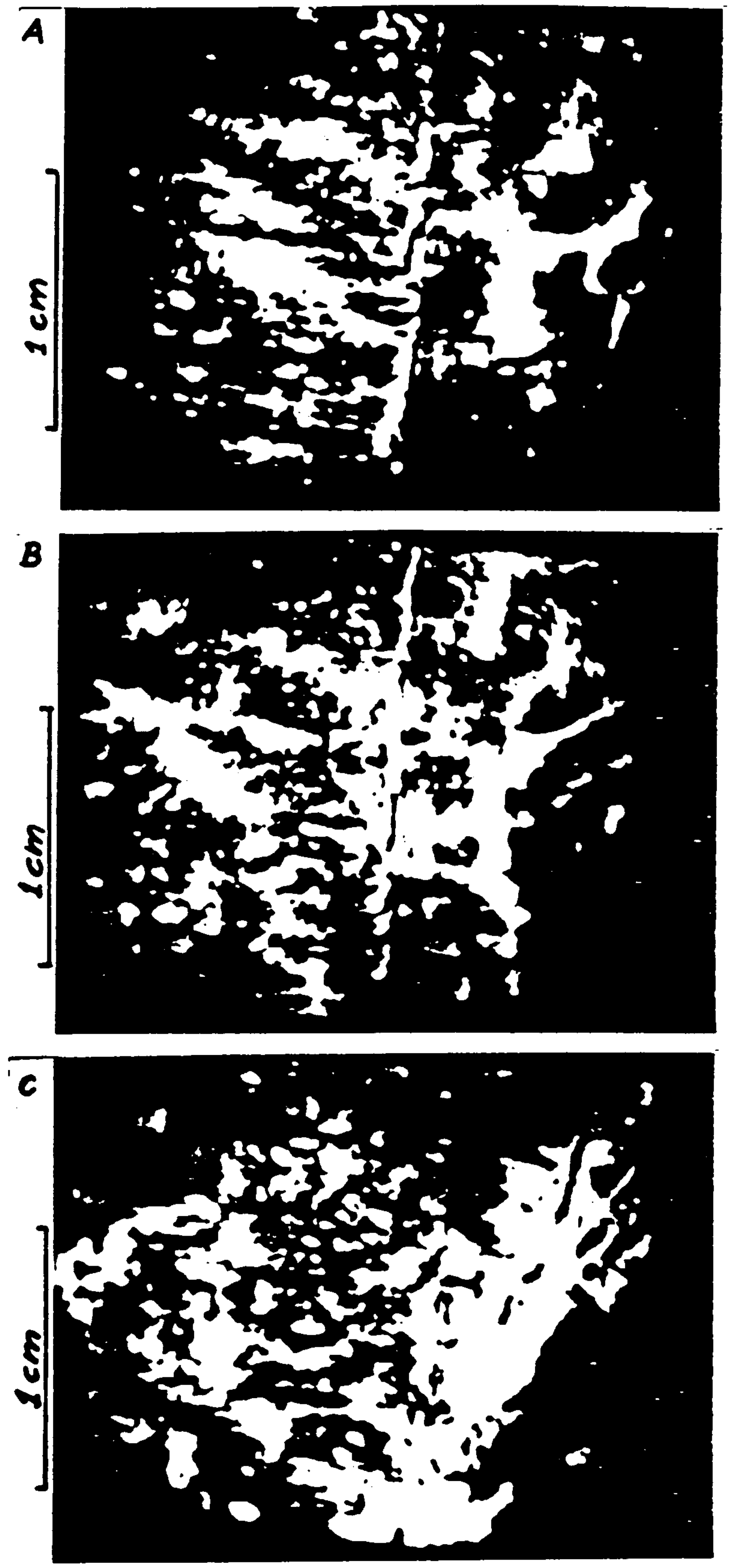

Figure 4. Schlieren images of solidifying off-eutectic (LiCl - 46.2mol% KCl) melt. Chilled from the righthand side. Visible distorted image of reference wire. Time of photograph reported in minutes from beginning of experiment: (a) 10.08, (b) 11.17, and (c) 15.42.

ORIGINAL PAGE IS
OF POOR QUALITY

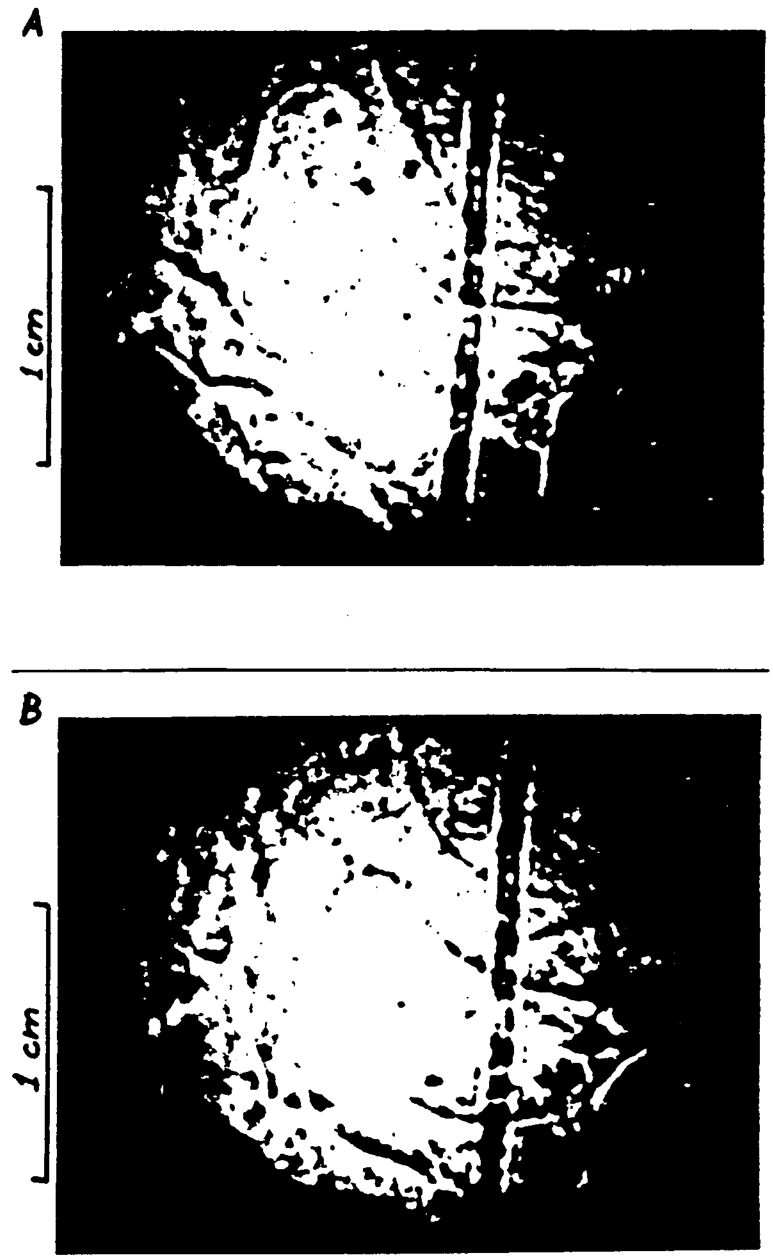

Figure 5. Shadowgraph of solidifying off-eutectic melt. Visible rising plumes caused by double diffusive phenomena. Chill placed beyond field of view to the right./ Time of photograph reported in minutes from beginning of experiment: (a) 20 and (b) 20.17.

Reference List

1. J.S. Langer, *Metall. Trans.* 15A (1984): 961.

2. M.E. Glicksman, R.J. Schaefer, and J.D. Ayers, *Metall. Trans.* 7A (1976): 1747.

3. S.R. Coriell, M.R. Coreles, W.J. Boettinger, and R.F. Sekerka, *J. Crystal Growth* 49 (1980): 13-28.

N89-13676

S5-76
175208
22 P.

Fluid Mechanics and Mass Transfer in Melt Crystal Growth: Analysis of the Floating Zone and Vertical Bridgman Processes

Principal Investigator: Professor R.A. Brown

MJ 700807

Summary

Fundamental understanding of the interactions of heat and mass transport, melt flow and the morphology of solidification interfaces are crucial to the design and interpretation of experiments aimed at microscopically controlled solidification of crystals on earth and in space. This research program focuses on analyses of the transport mechanisms in solidification processes, especially one of interest to the Microgravity Sciences and Applications Program of NASA. Research during the last year has focused on analysis of the dynamics of the floating zone process for growth of small-scale crystals, on studies of the effect of applied magnetic fields on convection and solute segregation in directional solidification, and on the dynamics of microscopic cell formation in two-dimensional solidification of binary alloys. The most significant findings have been:

1. The completion of the modification of our finite-element analysis of the thermal-capillary model for small-scale floating zones to include axisymmetric fluid flow in the melt driven by buoyancy differences, surface tension gradient and rotation of the feed and crystal rods.

2. Analysis of the effect of a vertically aligned applied magnetic field on buoyancy-driven convection and solute segregation in vertical directional solidification. Results are reported for specific crystal growth systems developed at MIT and Grenoble.

3. A study of the existence of a fundamental mechanism for wavelength selection in solidification of two-dimensional cellular interfaces from a binary melt based on large-scale numerical simulations has shown that steadily solidifying structures are possible for a **continuous range of wavelengths.** This results opposed results of model calculations for more idealized solidification systems where mechanisms for selecting a specific wavelength of the microstructure seem to exist.

4. The design and construction of an experimental system for the growth of two-dimensional microstructures is just about complete. This system is carefully designed for controlled, quantitative experimental measurements of interface morphologies over a range of operating conditions where theoretical predictions are available from our calculations.

Effect of Vertical Magnetic Field on Vertical Bridgman Crystal Growth

The successful prediction of interface morphologies and segregation in crystals grown by directional solidification involves complete solution of the macroscopic free-boundary problems that describe melt and heat flow, solute transfer and the melt/crystal interface morphology with accurate accounting of realistic heat transfer conditions for the particular furnace design. We have designed a numerical simulator for this purpose based on finite-element algorithms. Calculations from the simulations have been compared directly with experimental measurements for gallium-doped germanium growth in the apparatus built by A.F. Witt and MIT.[13] The agreement is remarkable, considering that no attempt has been made to adjust any of the thermo-physical properties. This work was highlighted in the 1985 annual report. In the last year we have extended the calculations in several ways. First we have incorporated the effect of an imposed axial magnetic field into the calculations to give accurate predictions of the intensity of the field needed to yield diffusion-controlled crystal growth on earth; this research has been submitted for publication and is highlighted below. Secondly, we have extended the finite-element simulations of directional solidification to include the transients associated with the batchwise nature of the system by solution of the time-dependent field equations and boundary conditions for the appropriate moving-boundary problem. The computer code for this effort is in the final stages of development and we will report in simulations and direct comparison with experiments in another report.

In recent years, steady-state magnetic fields have been imposed in melt crystal growth of semiconductor materials to control fluctuations in solute or impurity concentrations caused by chaotic convection in the melt. The action of the field is caused by the Lorentz force induced by the magnetic field when the melt has high electrical conductivity. Increasing the field strength decreases the intensity of cellular convection driven by buoyancy forces. Besides eliminating chaotic and time-periodic convection in large-scale systems sufficient intense magnetic fields decrease the intensity of convection to the point that the axial and lateral variation of the solute concentration in the crystal are affected. The alteration of the laterally-averaged (across the melt/crystal interface) axial concentration of oxygen is one of the primary advantages of using magnetic fields in Czochralski growth of silicon. It is becoming increasingly evident that the lateral uniformity of solute profiles may be adversely influenced by imposed magnetic fields.

Increasing lateral inhomogeneities by decreasing convection mixing is not unexpected. The transition in axial and radial solute segregation from unidirectional crystal growth in the absence of bulk convection to growth with intense laminar mixing is described schematically by the curves shown in Figure 1 in terms of the percentage radial segregation Δ_c, defined as the maximum difference in concentration across the crystal measured as a percentage of the local average, and by the effective segregation coefficient k_{eff} defined as

$$K_{eff} \equiv k \, \langle c \rangle_I / \langle\langle c \rangle\rangle \tag{1}$$

where $\langle c \rangle_I$ is the laterally-averaged concentration of a solute at the melt/crystal interface and $\langle\langle c \rangle\rangle$ is the volumetrically-averaged concentration in the melt. In directional solidification, diffusion-controlled growth with a planar melt/crystal interface leads to uniform radial distribution of solutes, i.e. $\Delta_c = 0$. If the melt is sufficiently long that the diffusion layer adjacent to the interface occupies only a small fraction of the total length, k_{eff} is unity in the absence of bulk motion other than the unidirectional growth velocity V_m. The length of the axial concentration gradient can be controlled, since the scale of the diffusion layer is set by the ration D/V_m. Curvature of the melt/crystal interface induces lateral solute variation caused by the focusing of the diffusion field adjacent to the interface.

Weak laminar convection distorts the one-dimensional concentration field and causes the radial and axial segregation indicated on Figure 1. When the mixing of a solute by these flow fields is in-

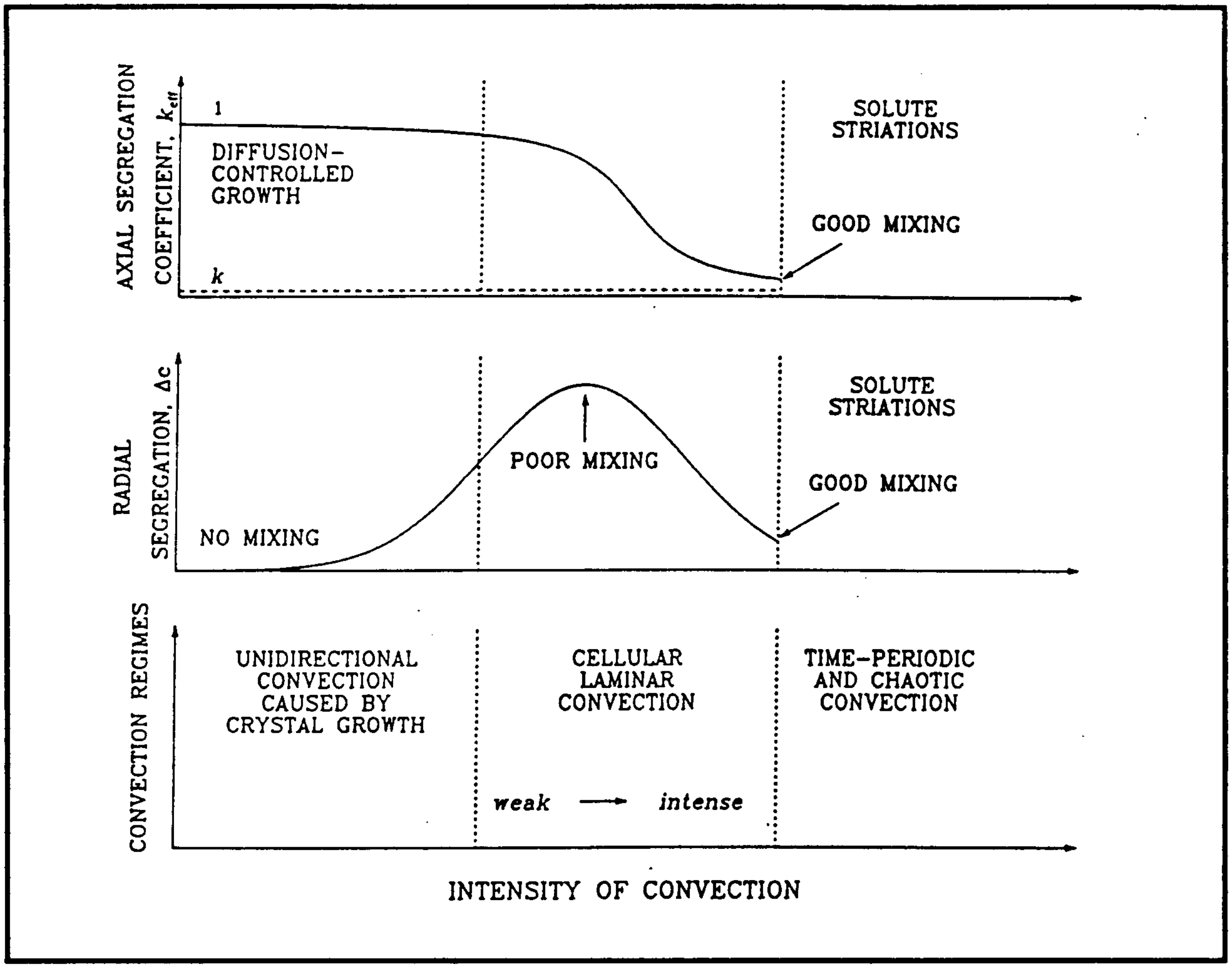

Figure 1. Schematic figure of the effect of flow intensity on the effective segregation coefficient and the percentage radial segregation in a directional solidification system.

complete its concentration field adjacent to the melt/crystal interface can be highly distorted and large amounts of radial segregation are possible, even when the axial composition profile indicate diffusion-controlled growth. Harriott and Brown[3] demonstrated the effect of weak convection caused solely by differential rotation of the feed and crystal rods on radial segregation in small-scale floating zones. This situation exists in well-controlled small-scale crystal growth experiments on earth, in the growth of nondilute binary alloys where the solute field damps convection, in microgravity experiments in which convection has not been stopped entirely, and in experiments with strong magnetic fields.

Solute boundary layers form adjacent to the melt/crystal interface when laminar convection leads to intense mixing. Then the radial segregation of solute decreases and the composition of the melt approaches a new bulk value elevated (assuming $k < 1$) by the mixing of the solute rejected at the interface. In the limit of very thin solute layers k_{eff} approaches k and the solute concentration increases steadily along the length of the growing crystal. Strong laminar convection is rarely found in the low Prandtl number melts of semiconductor materials. Instead time-periodic and chaotic transients in the melt lead to thermal transients near the interface and induce melting and accelerated crystal growth on the time scale for the fluctuation.

The purpose of our work has been to present detailed calculations of the action of a magnetic field on convection, segregation, and heat transfer in a realistic models for the vertical Bridgman crystal growth system and to quantify the intensity of the field that is necessary to achieve diffusion-controlled, unidirectional solidification in such systems. We have performed calculations for the furnace and ampoule designs for small-scale experiments used in the experimental studies of C.A. Wang (Ph.D. Thesis, MIT, 1984) and Rouzaud et al. (*J. Crystal Growth* 69, p. 149, 1985). The furnace of Wang is a classical Bridgman-Stockbarger system with isothermal hot and cold zones separated by an insulated region designed to create a constant axial temperature gradient in the melt and crystal adjacent to the solidification interface. The furnace of Rouzaud et al. uses a tapered heating element to establish a nearly linear temperature profile over a length of ampoule approximately 30 times the radius of the furnace. The furnaces in both systems are designed so that the crystal growth rate is equal to the ampoule displacement rate after an initial transient caused by the onset of ampoule motion.

Detailed calculations of the temperature fields, melt flow, and axial and radial segregation patterns for these two furnaces were determined for growth of dilute gallium in germanium in both systems without the presence of the magnetic field.[13] Both systems exhibited the transition from diffusion-controlled solute transport to laminar mixing with increasing thermal Rayleigh number. For the conditions of an earthbound experiment, the convection was intense, radial segregation was minimal, and the effective segregation coefficient approached the value of the equilibrium segregation coefficient. In this paper we quantify the levels of imposed magnetic fields necessary to damp this convection to the extent that low radial segregation without axial segregation ($k_{eff} \sim 1$) is obtained.

The calculation are based on the finite-element Newton method[14,13] for the solution of conservation equations and boundary conditions associated with the velocity, pressure, and solute fields in the melt, the temperature in melt, crystal and ampoule, and the shape of the melt/crystal interface. The extension of the method to accommodate the vertical magnetic field is trivial and has been previously described.[17] The abstract of the paper describing the method[17] follows:

> Effect of Vertical Magnetic Field on Convection and Segregation in Vertical Bridgman Crystal Growth, D.H. Kim, P.M. Adornato, and R.A. Brown, *J. Crystal Growth*, (submitted, 1987).
>
> The Petrov-Galerkin/finite-element analysis of vertical Bridgman growth for dilute and nondilute alloys presented before (*J. Crystal Growth* 80 (1986) 155) is extended to include the effect of a vertically-aligned magnetic field in the limit of zero magnetic Reynolds number. Calculations are presented fro growth of a dilute gallium-germanium alloy in a vertically stabilized Bridgman-Stockbarger system and in a furnace with a uniform temperature gradient imposed along the ampoule. Steady cellular convection driven by radial temperature gradients causes good axial and radial mixing in both systems without a magnetic field. A weak magnetic field decreases the intensity of convection and the effectiveness of solute mixing. The radial nonuniformity is greatest for an intermediate field strength. Stronger fields suppress flow recirculation completely and lead to uniform solute segregation across the crystal and to diffusion-controlled axial segregation.

Contours of the temperature, stream function (velocity) and concentration fields are shown in Figure 2 for the thermal Rayleigh number $Ra_t = 1\text{x}10^7$ without the magnetic field, i.e. the Hartmann number is $Ha = 0$. The radial temperature gradients are caused primarily by the differences in the thermal conductivities of melt, crystal and ampoule material and are largest adjacent near the convex melt/crystal interface. The temperature field and interface shape are essentially unaffected by the flow.

The two flow cells are driven by different sets of radial temperature gradients along the ampoule caused by interactions between the furnace and the ampoule. The differences between the thermal conductivities of the melt ($k_m = 0.39$ W/K cm), the crystal ($k_s = 0.17$ W/K cm) and the ampoule ($k_a =$

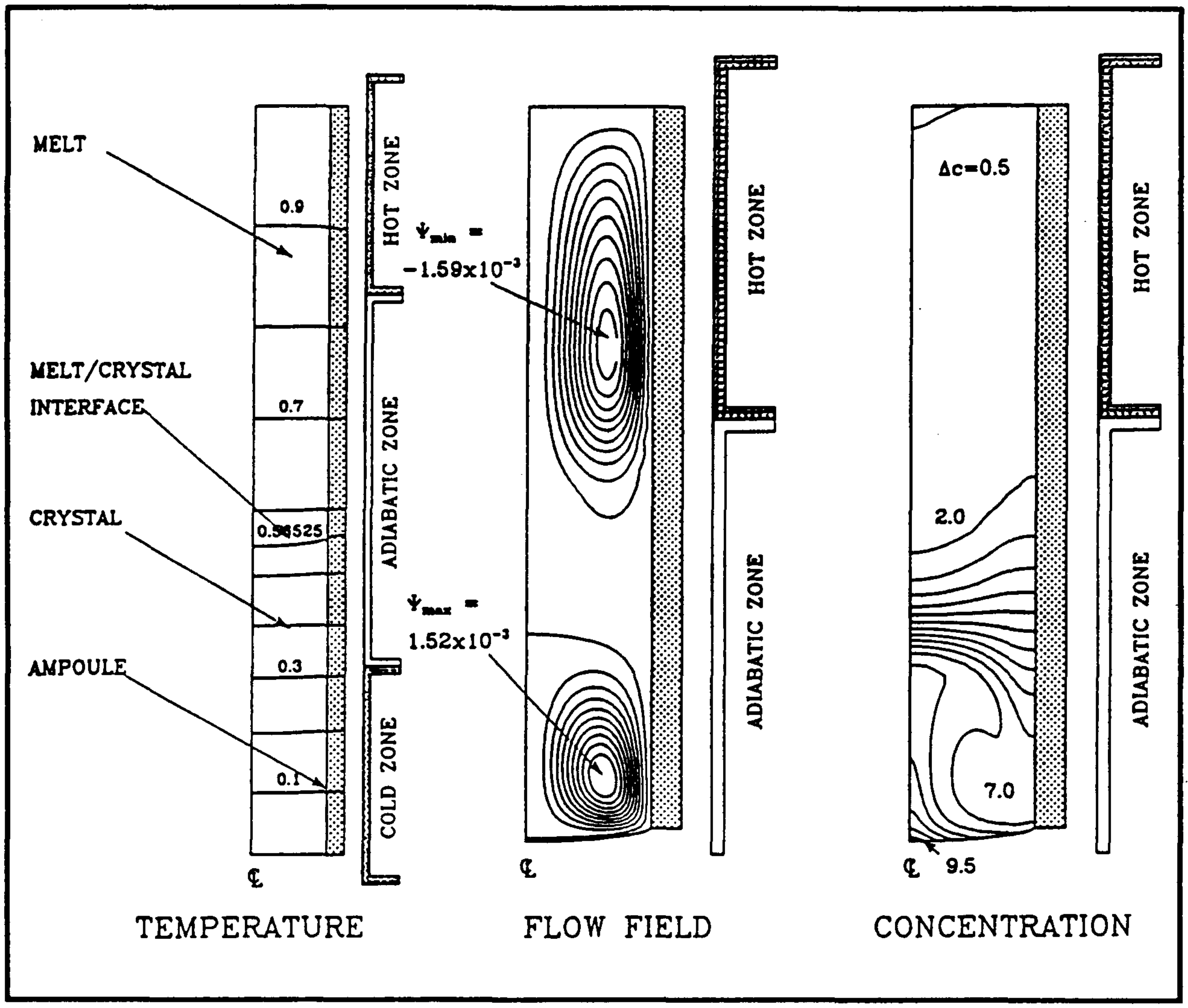

Figure 2. Contours of temperature, stream function, and concentration for growth in the vertical Bridgman furnace with V_g = 4 μm/sec and Ra_t = 1x10^7. Streamlines are spaced at equal intervals between the maximum (or minimum) values for the cells and zero.

0.26 W/K cm) cause the melt/crystal interface to be convex with respect to the melt and results in the temperature decreasing radially adjacent to this phase boundary. These gradients drive a flow that is up along the axis of the ampoule and down along the wall. Because of the slender shape of the melt, this flow is confined to a portion of the ampoule bottom that is on the order of the ampoule radius.

The mismatch in thermal boundary conditions between the adiabatic and hot zones of the furnace causes a second set of radial gradients with the hottest temperature located at the ampoule wall. The upper flow cell is driven by this part of the temperature field and moves upward at the wall and down along the centerline. The spacing between the two flow cells is controlled by the length of the adiabatic zone.

The gallium concentration field in Figure 2 shows the effects of the mixing caused by both the top and bottom flow cells. The radially uniform and exponentially decreasing concentration field expected without bulk convection is distorted in parts of the melt where either cell is strong. The concentration above the top of the adiabatic zone is essentially uniform because of the upper cell and because the diffusion layer would not penetrate into this portion of the ampoule, even at Ra_t = 0. The concentration field near the melt/crystal interface is deformed by the lower cell and the first stages of the formation of a region of uniform concentration are evident. Steep axial concentration gradients develop in the region of the ampoule between the two cells.

The temperature field and melt/crystal interface for $Ra_t = 1x10^7$ and Ha = 0 are essentially the same as predicted without convection in the melt ($Ra_t = 0$), mainly because of the low Prandtl number for the melt. Increasing Ha has essentially no effect on these variables.

The effects of the axial magnetic field on the flow field is shown in Figure 3. Very weak fields,

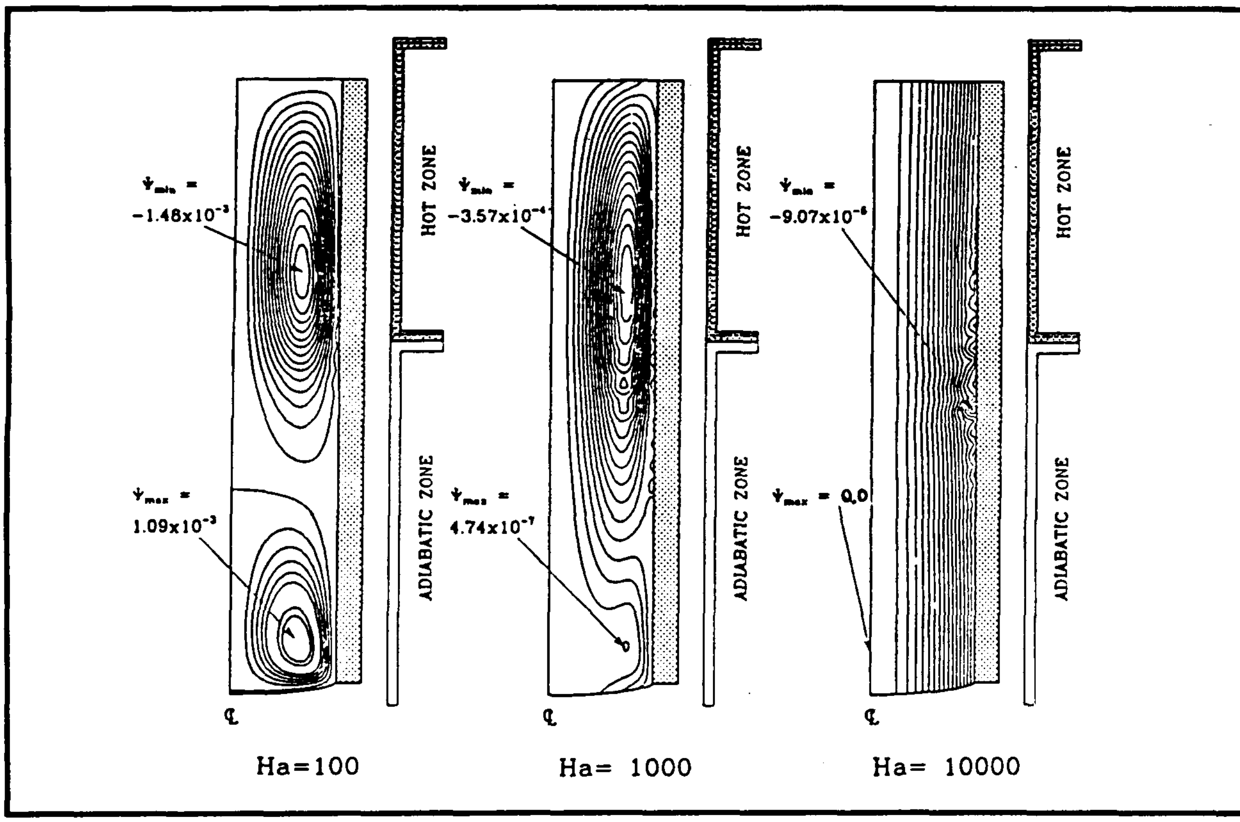

Figure 3. Sample flow fields for growth in the vertical Bridgman furnace with increasing magnetic field strength measured by Ha; $Ra_t = 1 \times 10^7$.

e.g. Ha = 10, decrease the strength of the flow, but leave the flow pattern unchanged. Increasing the field strength causes the flow cell to stretch to fill most of the ampoule, so that more of the flow is aligned with the field and hence unaffected by it. At Ha = $1x10^4$ the cell has disappeared and only the unidirectional motion due to crystal growth remains.

The small value of the solute diffusivity makes the solute concentration field much more sensitive to the level of convection than the temperature field. Solute fields for dilute gallium in germanium are shown in Figure 4, as calculated for the flows shown in Figure 3. The regions of approximately uniform concentration formed by mixing in the two flow cells are still apparent for Ha = 100. The disappearance of the lower flow cell with increasing Ha leads to the reformation of the exponential diffusion layer adjacent to the interface for Ha - $1x10^3$ with weak convective mixing caused. only by the upper flow cell.

The percentage radial segregation Δc is plotted in Figure 5 as a function of Ra_t and Ha for V_g = 4 μm/s. The maximum in Δc occurs for approximately $Ra_t \approx 1x10^6$. The value of Ra_t for the maximum radial segregation increases as the intensity of the field is increased. For Ha > $\geq 1x10^3$ Δc is caused

ORIGINAL PAGE IS
OF POOR QUALITY

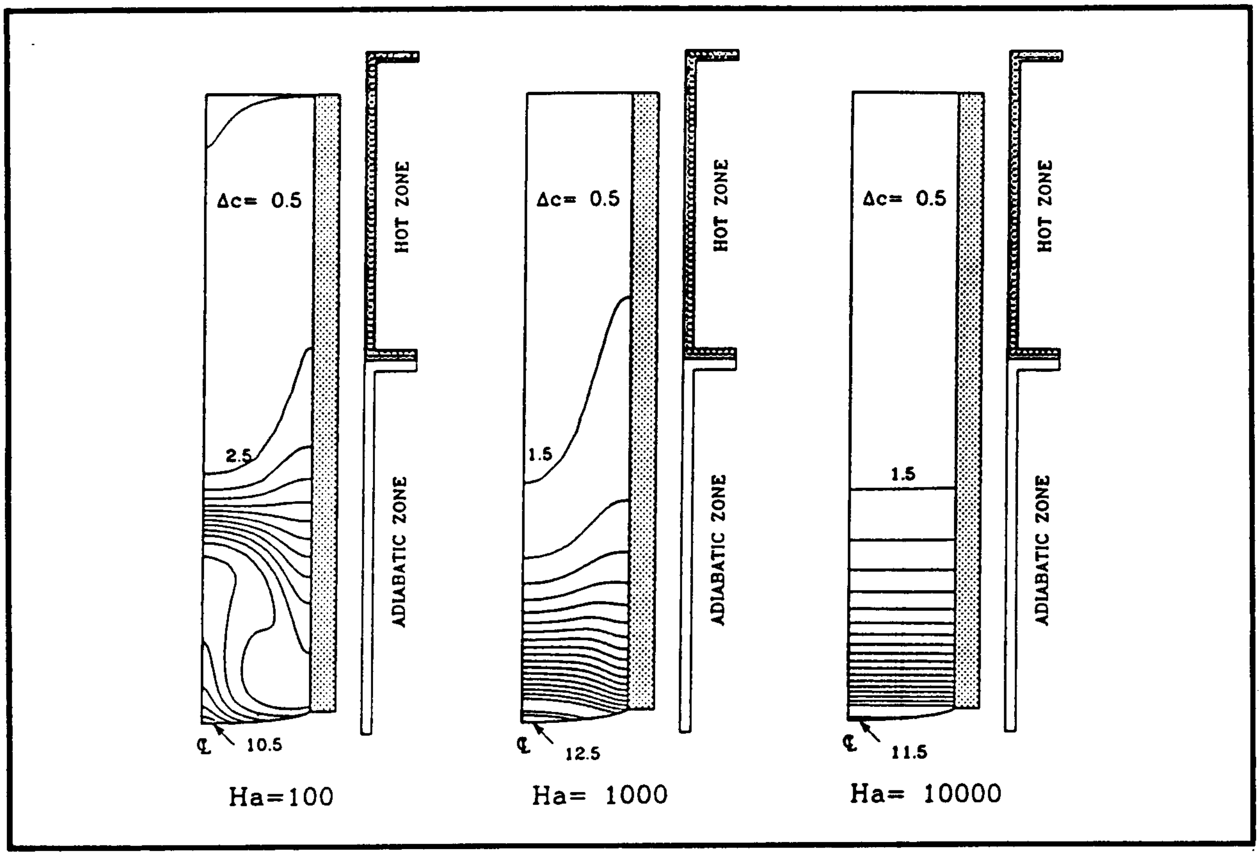

Figure 4. Sample gallium concentration fields for growth of GaGe in vertical Bridgman system with V_g = 4μm/sec as a function of Ha; $Ra_t = 1x10^7$.

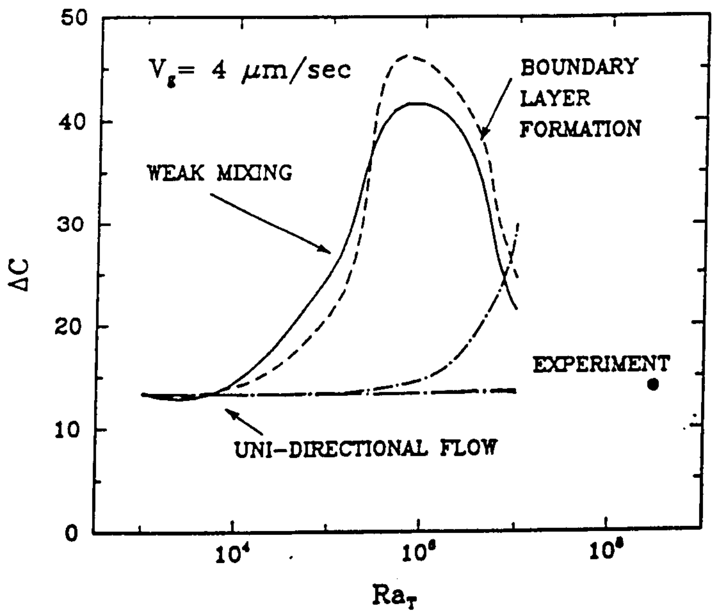

Figure 5. Percentage radial segregation as a function of thermal Rayleigh number and Hartmann number for growth of GaGe in the vertical Bridgman system with Vg = 4 μm/sec. The solid dot corresponds to experimental measurements of Wang.[17]

only the curvature of the melt/solid interface up to $Ra_t = 1x10^7$. calculations at higher values of Ra_t were not possible with the finite element mesh used here because.of the formation of the boundary. The experimental measurement of Wang also is shown; Adornato et al.[13] explained how to extrapolate the numerical calculations to get reasonable agreement with these measurements by using boundary-layer theory for describing the dependence of Δc on Ra_t.

The variation of the axial segregation of solute can be estimated from the calculations with the PSSM by computing the effective segregation coefficient defined by Equation (1). These values are plotted in Figure 6 as a function of Ra_t and Ha. The value of k_{eff} for low convection (Ra_t - 0) is not

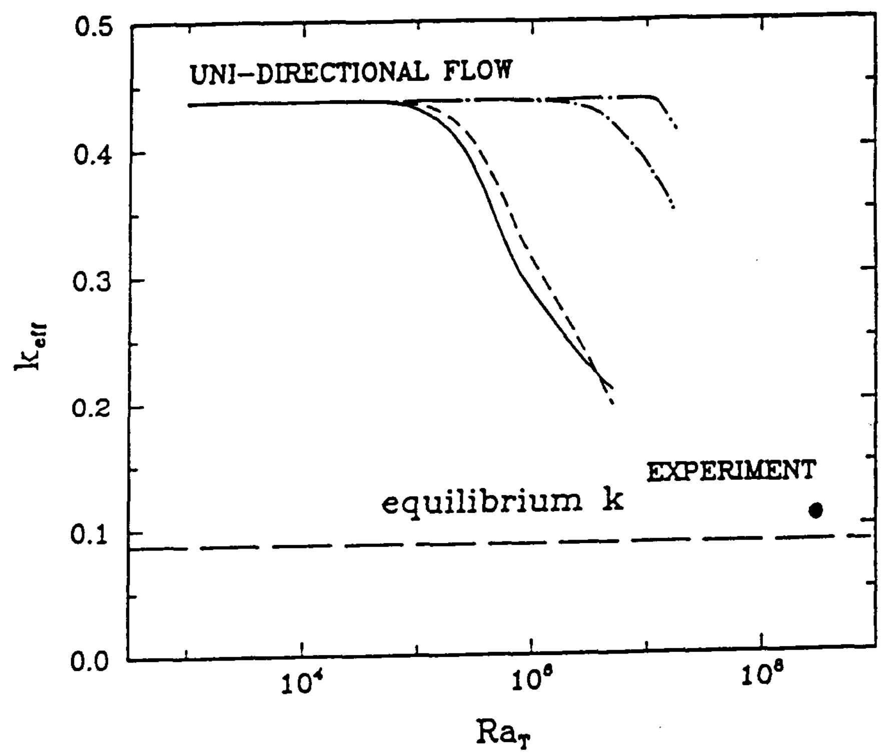

Figure 6. Effective segregation coefficient computed from equation 1 as a function of Ra_t and Ha for growth in vertical Bridgman furnace with V_g = 4 μm/sec. The solid dot correpsonds to the experimental measurement of Wang.

unity because the ampoule is not long enough for the variation in concentration caused by the diffusion layer to be small relative to the portion of the melt which is at the bulk concentration (c = 1). The increased mixing caused by convection and the decrease in k_{eff} towards the equilibrium value (k = 0.087) are obvious. Increasing the magnetic field strength increases the effective segregation coefficient, shifting the critical value of Ra_t for the beginning of the decrease in k_{eff} to higher values. The experimental measurement of Wang without a magnetic field is again shown for reference.

Direct comparison between these calculations and experiments with strong magnetic fields are underway. The experimental data is being supplied by Prof. A.F. Witt through research also funded by NASA.

Microscopic Modelling of Pattern Formation in Two-Dimensional Solidification

Morphological stability theory describes the mechanisms for a smooth solidification front separating a binary melt form its solid to develop undulations that lead to cellular and dendritic structures on the microscale. Although the onset of morphological pattern formation is well understood from linear stability theory pioneered by Mullins and Sekerka, the transitions to deep cellular and dendritic structures are not. Our theoretical and experimental program is aimed at this goal for two-dimensional, thin-film solidification experiments where quantitative experiments are possible.

We have developed asymptotic and numerical methods aimed specifically at analysis of pattern formation in two-dimensional solidification experiments. The development of these techniques is discussed in a number of our publications[5,16]. The results from several recent publication are discussed in the following section on the theoretical analysis of two-dimensional solidification. Our research program has expanded from a purely theoretical and computational effort to the development of a precise experimental system for studies of two-dimensional solidification, as analyzed by our calculations. This system was developed during this year of NASA support and is outlined in the section entitled "Experimental System".

Theoretical Analysis of Two-Dimensional Solidification

Analysis in the previous year has focussed on two aspects of microscopic pattern formation in two-dimensional solidification. First, is an explanation for the lack of experimental observation of the spatial wavelength for small-amplitude cells predicted by linear stability theory, as reported by a number of experiments in recent years. The second issue is the transition to deep cellular patterns and the possibility of a mechanism for selection of a specific spatial wavelength from the large range of linearly unstable ones. Each of these issues is discussed in the review paper abstracted below:

> "Numerical Analysis of Cellular Solidification Microstructures," R.A. Brown, N, Ramprasad, M.J. Bennett, *Supercomputers in Chemistry and Chemical Engineering* ACS Symposium, eds. K. Jensen and D. Truhlar (ACS, 1987).
>
> Large-scale numerical calculations are used to simulate the formation of cellular microstructures during directional solidification of a binary alloy. The analyses are based on finite-element methods developed especially for solving the free- and moving-boundary problems that describe the solute field in melt and solid and the melt/solid interface shape in the Solutal Model of microscopic solidification. Calculations are reported for individual cells that show the transitions from steady-state solidification of shallow cells bear the onset of morphological instability to deep cells separated by narrow grooves as seen in experiments. Simulations with multiple cells show the importance of nonlinear interactions between shapes with resonant spatial structures in determining the time-dependent dynamics of large collections of cells. The results of cellular dynamics calculations fro multiple cells show the possibility of long time-scale time-periodic and quasi-periodic interactions.

Analysis of nonlinear transitions in shallow and deep, two-dimensional cells are discussed separately below.

Nonlinear transition for shallow cells

The key feature of directional solidification systems which leads to the complex nonlinear interactions seen experimentally is the flatness of the small surface energy associated with the melt/crystal interface. Since the surface energy is the sole effect which stabilizes a planar interface against short wavelength instabilities, the resulting neutral stability curve for the onset of cellular growth is extremely flat. This is seen in Figure 7, for a set of thermophysical properties similar to PbSn, except that the solute diffusivity in melt and solid is taken to be the same. Note that approximately the same value of the growth rate $V_c(\lambda)$ leads to instability for a band of wavelengths which stretches over an order-of-magnitude. This flatness of the neutral stability curve leads to nonlinear interactions between spatial resonant values of the wavelength lower than the critical value predicted by linear

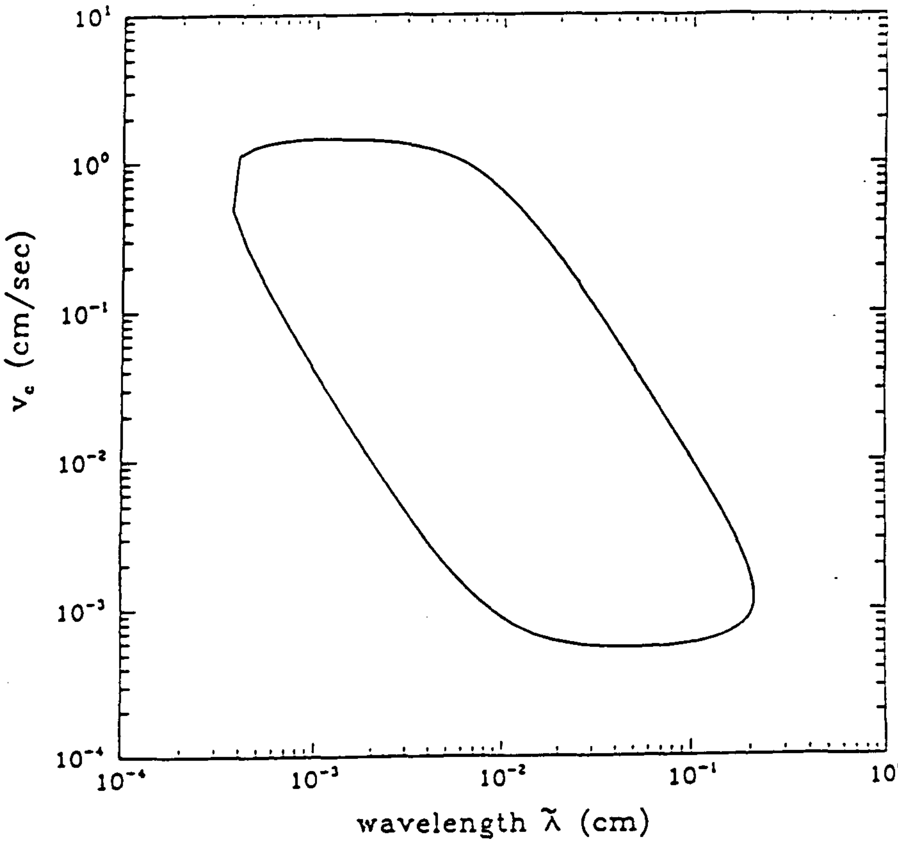

Figure 7. Neutral stability curve predicted from linear analysis for values of the thermophysical properties appropriate for PbSn, buth with equal diffusivities in melt and solid.

theory, as observed in the experiments. The theoretical development of this observation is given in the reference below along with detailed nonlinear calculations:

> "Nonlinear Interactions of Interface Structures of Differing Wavelength in Directional Solidification," M.J. Bennett, R.A. Brown, and L.H. Ungar, Proceedings of the International Symposium on the Physics of Structure Formation (Springer-Verlag, 1987).

> **The solution structure of the cellular patterns formed during the directional solidification of a material containing a dilute impurity is studied by numerical analysis of a simple model. Solution families corresponding to cells of different spatial wavelength arise as the growth velocity is increased above the value for the onset of the instability. The resonant interaction between these steady-state shapes leads to both stable and unstable time-periodic oscillations. Only some of the oscillatory interface structures computed have been predicted by normal mode analysis of codimension-two bifurcations. The interactions between cells with different spatial structures limit the range of validity of asymptotic expansions to a velocity range too small to be reliably measured experimentally.**

The nonlinear transitions caused by these codimension-two bifurcations are demonstrated in Figure 8 by calculations of cells with specific wavelengths as a function of the dimensionless growth rate $P \equiv V\lambda/D$, where D is the solute diffusivity. The thermophysical properties for these calucations are the same as used in the calculation of the neutral stability curve, Figure 7; the sample size $\lambda_c = 4.5$ correpsonds to the most unstable wavelength predicted from this figure. Nonlinear cell shapes with

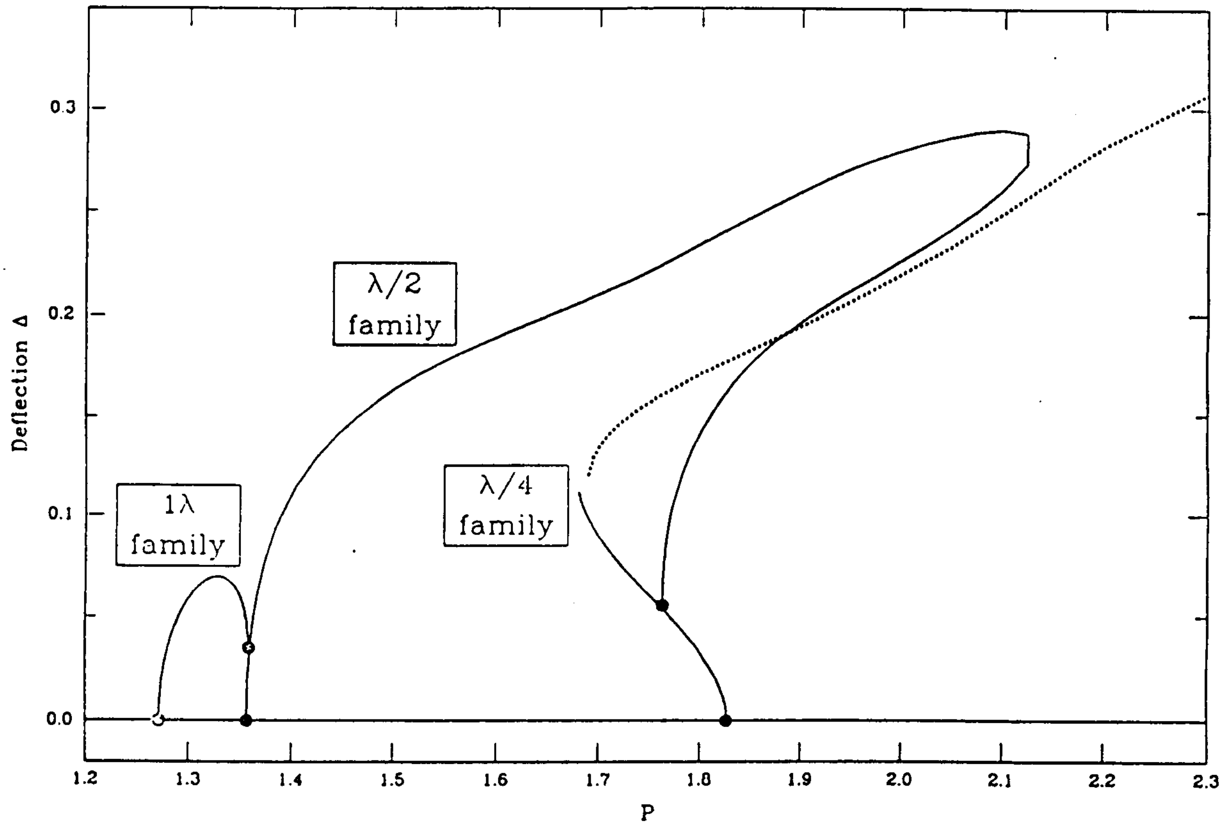

Figure 8. Families of steady-state shapes computed as a function of increasing growth rate P in a $\lambda_c/2$ sample size.

this wavelength evolve from the critical value $P = P_c(\lambda)$ predicted by linear theory. Two secondary bifurcation points are computed for $P < 2P_c\,(\lambda_c)$ which reduce the wavelength of the computed cell shape to $\lambda_c/4$. The amplitude of the cells is represented by the dimensionless cell depth defined as

$$\Delta \equiv \Delta/\lambda \qquad (2)$$

where Δ is the dimensional value and λ is the dimensional cell wavelength. Representative cell shapes are shown in Fig. 9 to demonstrate the steepening of the cell shape with increasing Peclet number. Calculations with the Monge interface representation were stopped because of the possibility that the interface would become reentrant, signifying that the solid melts and then resolidifies in the groove.

Figure 9 shows interface shapes computed using this representation with fixed wavelength $\lambda = 1$ and increasing P. The long cells have a distinct three-region structure with a rounded tip, a long sidewall and a small bottom. Increasing he Peclet number lengthens the sidewall relative to the other regions, and suggests an asymptotic structure.

We feel that the dynamics of wavelength selection for shallow cellular interface structures is best described as a statistical average of the dynamical behavior of a collection of cells over a long time. We are pursuing this approach through cellular dynamics calculations.

Wavelength Selection in Large-Amplitude Cells with Finite Depth

The calculations discussed above lead to the conclusion that no mechanism exists for selection of a specific spatial wavelength for shallow cells near the onset of pattern formation. To test for the

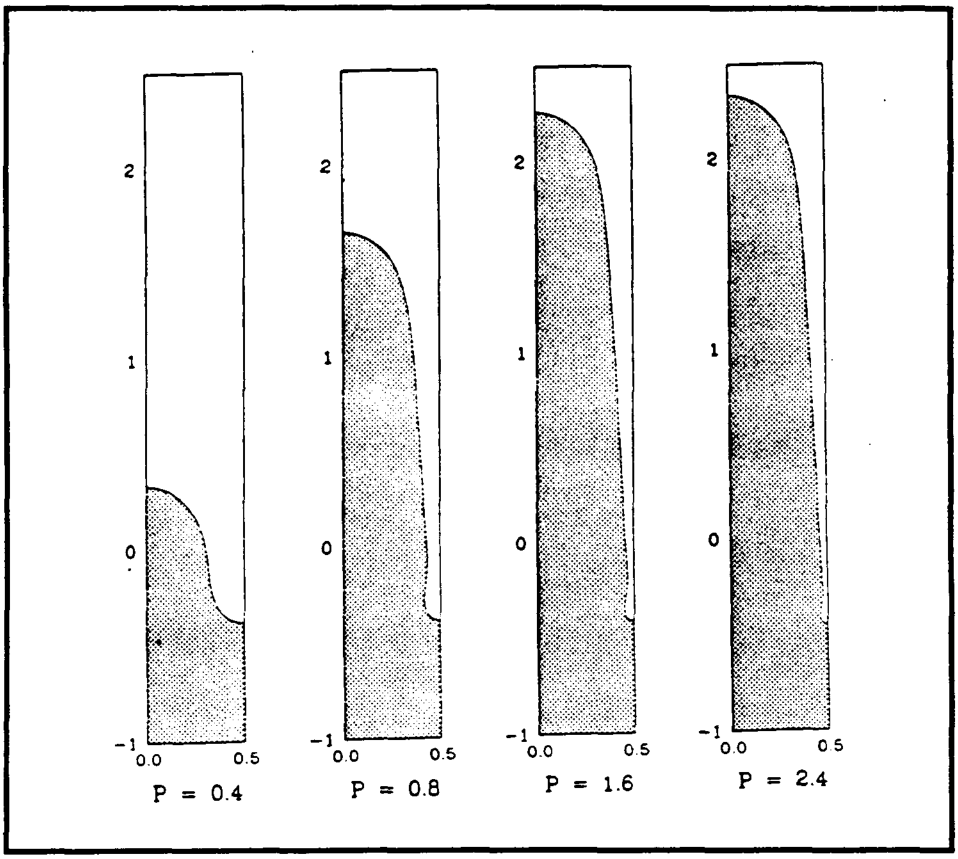

Figure 9. Sample interface shapes for increasing P and $\lambda = 1.0$ as computed with the method described by Ungar and Brown.[6]

existence of a mechanism for wavelength selection calculations for relatively deep cell. The abstract of the paper based on these calculations is given below.

> "Wavelength Dependence of Cells of Finite Depth in Directional Solidification," N. Ramprasad, M.J. Bennett, and R.A. Brown, Phys. Rev. A. (submitted, 1987).
>
> Finite element calculations are presented for individual shapes in a spatially period pattern of two-dimensional cellular interfaces that occur during the directional solidification of a binary alloy. The transition from shallow sinusoidal cellular shapes to cells separated by deep grooves is computed as a function of the spatial wavelength of the pattern as the growth rate is increased. The flatness of the neutral stability curve is responsible for secondary bifurcations that result from nearby codimension-two critical points. Tip splitting of the cells results and the apparent wavelength decreases by multiples of two from the value predicted by linear stability theory. Deep cells with rounded tips, linear sidewalls and pendent shaped bottoms are computed for a range of spatial wavelengths and growth rates, so that no mechanism for singling out discrete wavelengths is apparent. A wavelength corresponding to the cell with maximum depth is predicted as a function of the growth rate.

Figure 10 shows these calculations. The velocity is constant along each curve and is reported as a multiple of the critical value for the most dangerous wavelength $V_c(\lambda_c)$. Along each curve G and P decrease and Γ increases as λ is lowered. An important feature is that for each growth rate there is a deepest cell and this cell occurs for a decreasing value of the wavelength with increasing growth rate. For growth rates as low at (1.9) $V_c(\lambda_c)$ this maximum occurs at wavelengths less than $\lambda = 1$, compared to $\lambda_c = 4.5$. This is not unexpected, because the wavelength splitting mechanisms demonstrated in

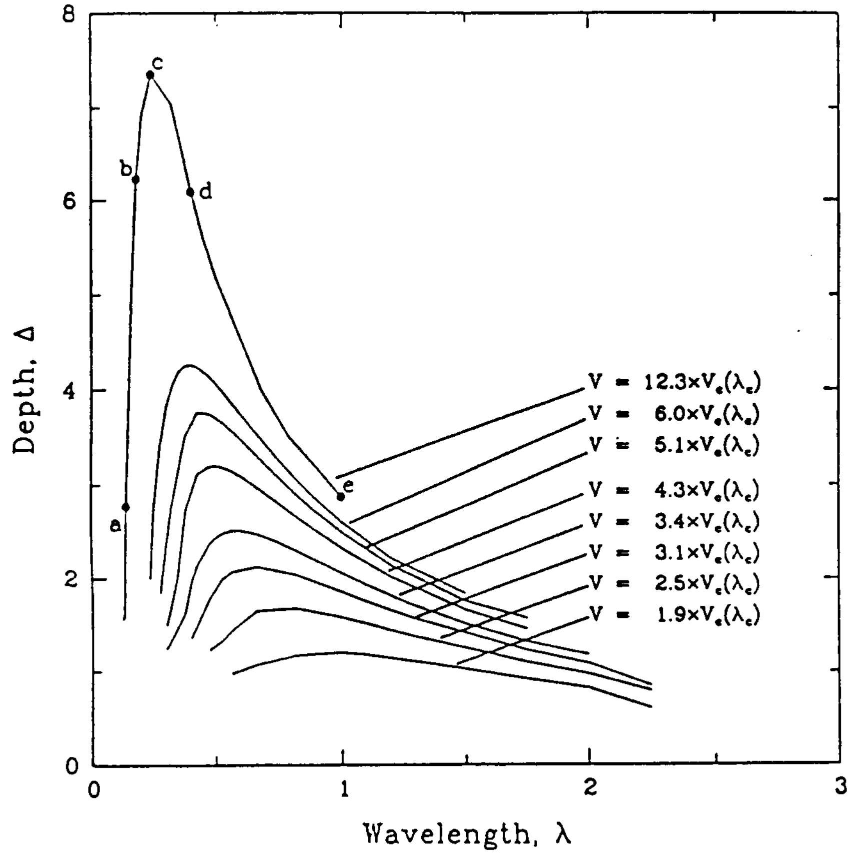

Figure 10. Dependence of cell depth on wavelength for specific values of growth rate P and other parameters held fixed.

Figure 10, indicate rapid transitions to shorter wavelengths. Deep cells ($\Delta > 2$) are computed within an increasingly narrower band of spatial wavelengths as the growth rate increases. This is an important observation because it gives evidence that some wavelength selection toward smaller values of λ does occur when the transitions from shallow cells to ones separated by deep grooves is considered.[19]

Sample cell shapes for varying wavelengths along the curves with the highest growth rate are shown in Figure 11 rescaled so the lateral dimension of each cell varies between zero and one. The top and bottom of the cell shape for the shortest wavelength (11a) are extremely rounded, showing the dominant influence of surface energy in these regions. Calculations cannot be continued to lower values of λ using the mixed cylindrical/cartesian representation.[19] As the cell lengthens with increasing λ, a long sidewall or groove forms that separates the tip from the bottom. The interface shape and the axial variation of the concentration field are linear along the sidewall, showing that the contributions from the temperature field and the liquidus curve dominate the Gibbs/Thomson equation and that surface energy contributions are unimportant in this region. The cell bottoms are self-similar with increasing λ, but decrease in size relative to λ, because the capillary constant decreases proportional to λ.

The calculations for a single deep cell, but with a bottom suggests that adequate modelling of the dynamics of real cells probably must account for more detail of the cellular structure than is currently being considered in studies of idealized problems. Because of the finite length of these structures, the small surface energy seems to be controlling the length of the cell and selection of the wavelength through interactions that involve the matching of regions of the shape, like the tip and the sidewall

Figure 11. Cell shapes for representative calculations from Figure 10 and the highest growth rate. The letters for these shapes correpsond to the points shown on Figure 10. the wavelengths have been normalized so that the aspect ratio of the cells, measured as Δ, can be compared directly.

where it is relatively unimportant with the highly curved cell bottom. There is some hope that this structure can be captured by asymptotic analysis for simple solidification models; large-scale calculations are playing an important role in developing such a theory. A similar relationship may exist between the shapes of the tip and the sidebranching along a freely growing dendrite in directional solidification.

Experimental System

We have developed a quantitative thin-film solidification experimental system using the succinonitrile-acetone system, video imaging, digitization, and statistical data analysis to provide the framework for direct comparison with the calculations described above. The experiments differ from those performed previously in several important ways which will remove the ambiguities from the measurements:

a. Care is taken to control the pull rate within 1% of the critical value.

b. A **long** sample is used to insure that transients have decayed and that there is ample time for statistically meaningful data acquisition.

c. The video imaging system will lead to quantitative date on both the local cell shape and statistics on the cell front.

A. Solidification System

The solidification system designed for this experiment consists of long glass plates held in place by a metal support, as shown in Figure 12. The alloy is loaded into the sample through fill ports at either end. The sample is attached to a translating stage (Control Technics Corporation) which is surrounded by a thermal environment constructed from hot and cold water baths separated by a nearly adiabatic region. The sample can be translated through the temperature field at rates between 1 and 100 μm/s at an accuracy of ± 0.1 μm/s, as set by the accuracy of the translation device. Although this accuracy is far better than previous experiments, it is not sufficient to support growth rates as low as

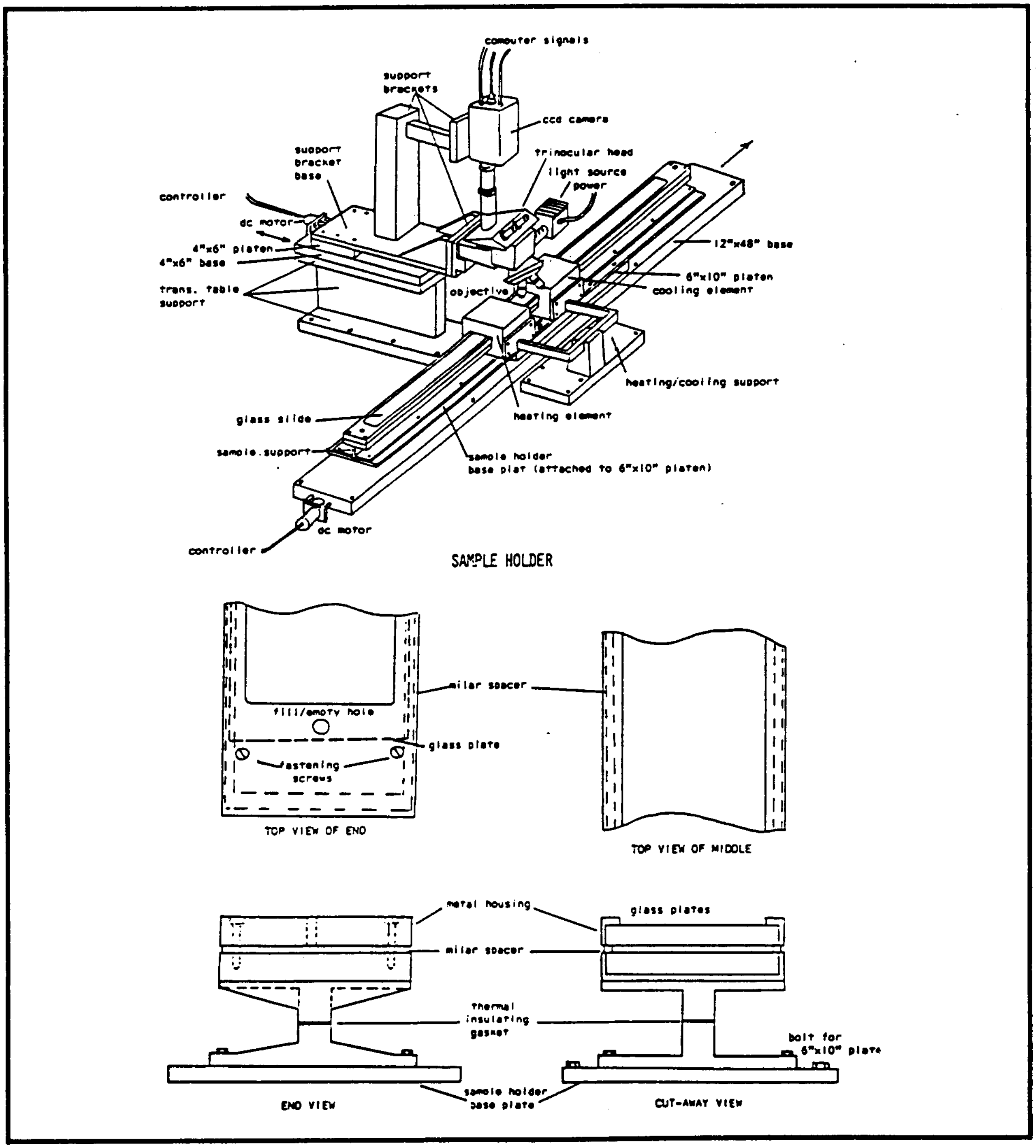

Figure 12. Schematic of proposed thin-film solidification system: (a) total system and (b) sample holder.

1.0 μm/s, as have been use previously where significant nonlinear interactions along the front are predicted to occur P less than 5% beyond P_c. We plan to use lower concentrations and higher growth rates so that the growth velocity can be control accurately enough to distinguish the nonlinear transitions.

The sample optical microscope is mounted to the lateral component of the translation stage so that the entire solidification front can be traversed. The translation system and furnace have been sized so that a sample <u>100 cm long</u> can be accommodated. This length is necessary for comparison with the long time scale evolution of shallow and deep cells predicted by the dynamical calculations to date and to gather time-dependent statistics for making quantitative measurements of possible chaotic interactions.

B. Alloys

Initial experiments will be conducted using the succinonitrile-acetone alloy. We have chosen this system because its thermophysical properties are extremely well characterized an because the alloy is chemically stable for long time periods. We plan to purchase the succinonitrile from Prof. Glicksman at RPI. Marginal stability curves for this alloy are shown in Figure 13 as a function of the

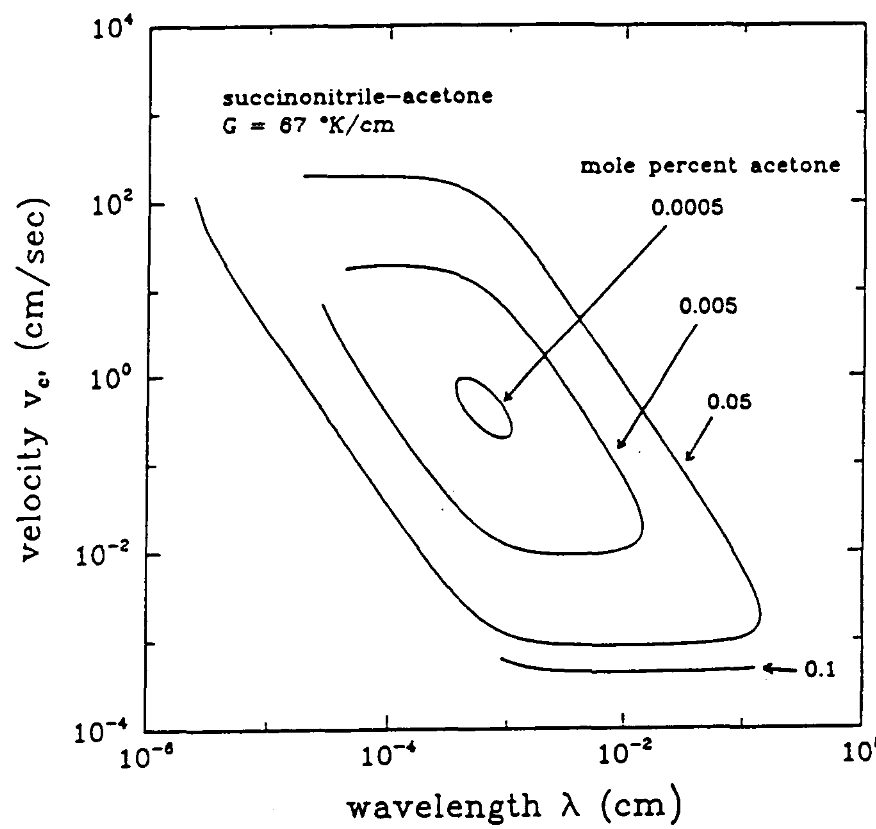

Figure 13. Neutral stability curves for succinonitrile-acetone system as a function of acetone concentration for fixed temperature gradient of 67°/cm.

acetone concentration. By decreasing the acetone concentration; to 0.01-0.05 mole %, the growth rate at the onset of instability can be increased to over 10 μm/s and the range of unstable wavelengths can be decreased significantly; compare the lateral extent of the curves for decreasing concentration. We expect the number of interacting wavelengths to decrease with decreasing concentration, so that steady-state forms are easier to obtain.

The need purity of succinonitrile is attainable by a combination of vacuum distillation and zone refining, as outline by Huang and Glicksman (Acta Metall. 29, p. 701, 1981). Purities of up to 99.9999% have been reported by these authors. Introduction of impurities during the loading of the sample will be avoided by hermetically joining the purification apparatus with the sample holder. The acetone will be added during the filling of the sample.

C. Data Acquisition and Analysis

A CCD camera fitted to a microscope with a 5-50x objectives is used to gather video images of the cellular interface, with approximately ten cells being viewed. Video images of the cellular front from the CCD camera are to be simultaneously recorder with a video recorder and processed through a Recognition Technologies Inc. (RTI) image processing system. This system will be configured to perform edge enhancement and recognition of up to 30 gray scale images (512x512 pixels) per second using software provided with the system. Because we expect the microstructure to evolve slowly in time (the growth of one wavelength of interface will take about 60 seconds), the RTI system should supply amble computational power for simultaneous analysis of the cellular structure within four laterally adjacent view ports for the objective, as controlled by the lateral translation of the stage, so that the dynamic interactions of approximately **forty** cells can be monitored.

Data in the form of the spatial locations of points along the interface will be passed into an IBM AT computer for storage and post-processing. The computer also controls the growth rate of the sample and the lateral location of the microscope objective. The data will be analyzed in several ways:

1. The melt/solid interface will be reconstructed and compared to the stored video images. This numerical form of the experimental data can be used for comparison with the asymptotic and numerical analyses described above.

2. Statistical information about the time evolution of the microstructure will be develop[ed by performing Fourier analysis on the interface shaped and computing correlation functions as a function of time. Software is available from RTI for these purposes. Simple quantities like the spatially-average wavelength as a function of time will be available as a result of this analysis. The correlation functions will give a direct indication of whether the interpretation of this average as a unique wavelength for the microstructure is meaningful.

Analysis of Small-Scale Floating Zone Systems

The reduced gravity environment of an experiment in space helps overcome considerable limitations to the floating zone process for growth of single crystals that exist on earth and make the study of this system of considerable importance to NASA's microgravity program. We have developed a detailed thermal-capillary model of the transport phenomena and interfacial phenomena important in small-scale floating zone systems. A schematic of this system is shown in Figure 14. Here a cylindrical rod of polycrystalline material is melted and resolidified into a single crystal by using a short circumferential radiative heater that translates slowly along the axis of the rod. The molten zone forms between the crystal and the feed rods and is held in place by surface tension. Its size is governed by heat transfer and limited by instabilities that have been assumed to originate at the meniscus. The radius of the rod is limited by the interaction of gravity with the shape of the meniscus and with heat transfer. We have developed a thermal-capillary model that accounts for these couplings and so can predicted operating conditions for small-scale floating zones. The model has been developed in two steps Figure 14 shows a schematic of a small-scale floating zone heater by a source with a Gaussian distribution.

First, a conduction-dominated model was described[18] that included the effects of the couplings between heat transfer and zone shape, but neglected convection in the so that the major heat transfer mechanisms modelled were conduction in each phase and radiation between melt and solid and the surroundings. Numerical solution of the free-boundary problem which describes the temperature field in each phase, the shapes of the two melt/solid interfaces and the meniscus has been by a

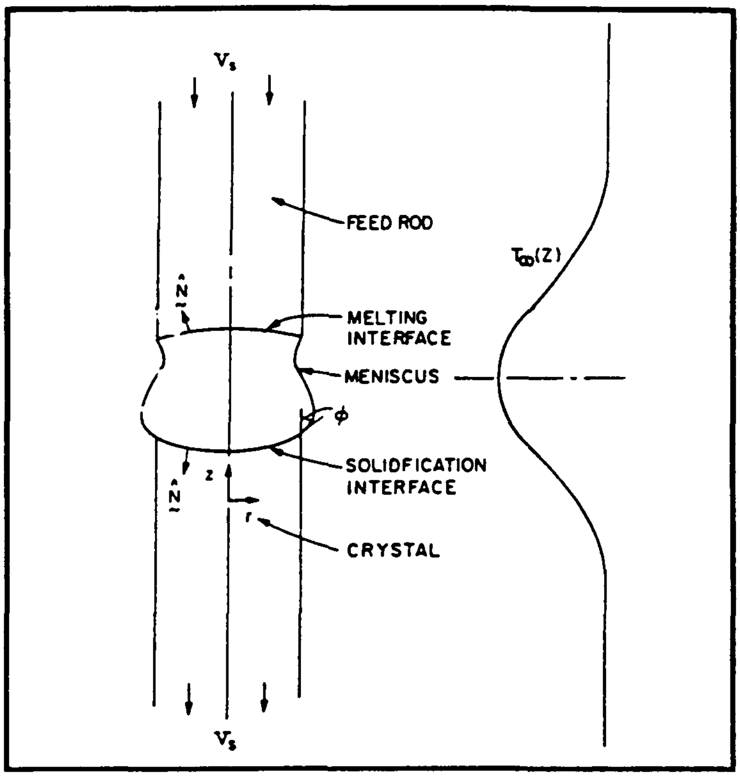

Figure 14. Schematic of small-scale floating zone system.

Galerkin finite-element method combined with Newton iteration which simultaneously compute corrections for all these variables. The development of this model, the numerical method and predictions for small-scale.silicon zones were described in a previous publication.[12]

Research in the last year has focussed on extending the analysis to include a description of fluid flow in the melt driven by buoyancy forces, surface tension gradients and rotation of the feed and crystal rods. The step is necessary to allow prediction of operating states for larger scale zones and materials with high Prandtl numbers, e.g. oxides, where convection in the melt is an important mechanism for heat transfer.

Incorporation of the fluid mechanics of the melt into the analysis has been straightforward, but tedious task. A mixed finite-element approximation to the velocity and pressure fields in the melt have been added along with Galerkin approximations to the momentum equation with the Boussinesq approximation and to the condition for incompressibility. These additional equation have been incorporated directly into the Newton iteration used in the conduction-dominated thermal-capillary model. The size of the matrix problem that must be solved at every Newton iteration has increased enormously; 2000 variables are typical for the conduction-dominated model, whereas 25,000 are needed for accurate approximations that include realistic flow in the melt. To do this has required the development of an out-of-core equation solver especially for the structures matrices that arise in application of Newton's method to free-boundary problems.

The testing of the finite-element code for solution of the thermal-capillary model with convection is just complete and simulations of specific growth systems, e.g. silicon, are underway. These results, as well as the development of the finite-element technique, will be reported later. This report only includes one example of calculations with this program to demonstrate the intensity of convection in even small-scale floating zones.

The flow fields appropriate for surface-tension driven flows in a self-consistent model of a 1 cm. radius silicon floating zone is shown in Figure 15 as a function of the Marangoni number, which is de-

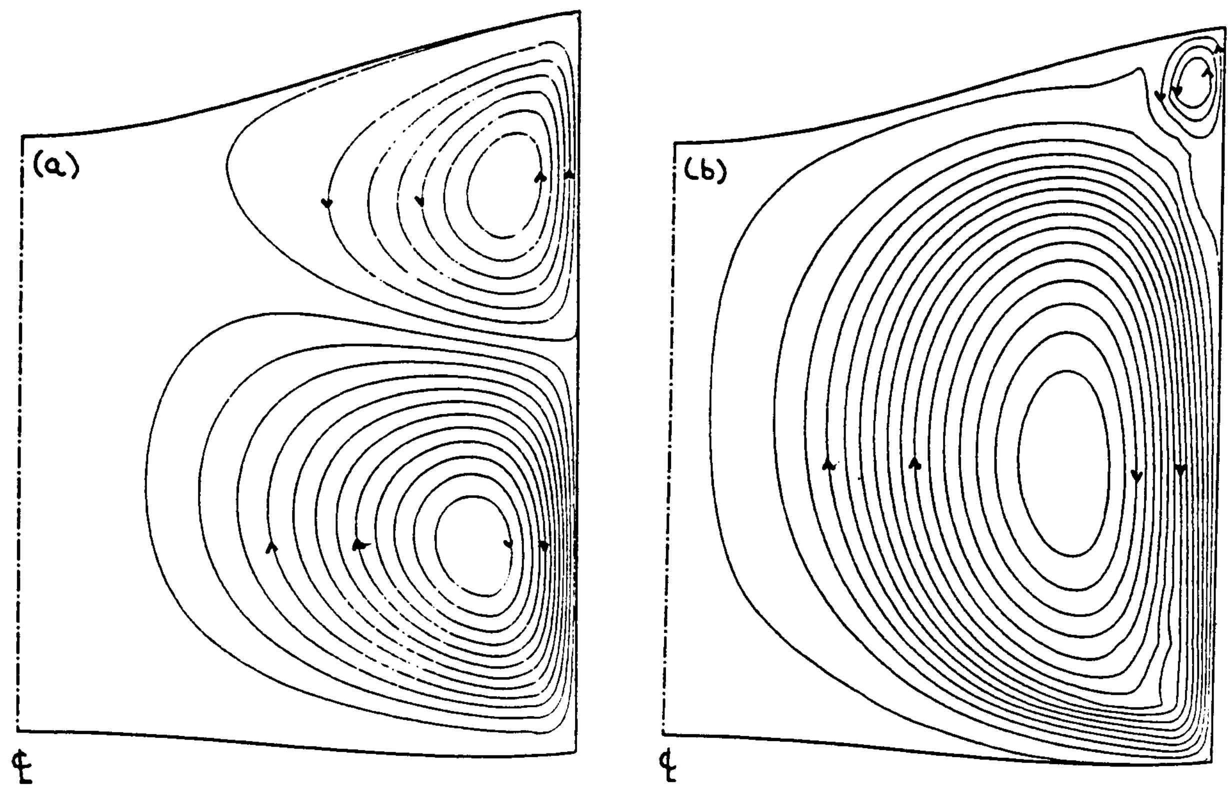

Figure 15. Stream function representation of flow patterns driven by surface-tension gradients for a small-scale silicon floating zone: (a) Ma - 100 and (b) Ma - 1×10^4.

fined here as Ma $\equiv (\partial\sigma/\partial T)T_m R/\alpha\mu$; values close to 1×10^6 are appropriate for silicon. The shape of the meniscus has been idealized in these calculations as a cylinder by setting the gravitational acceleration to zero and the wetting angle between the melt and crystal to 90°. The stream function contours plotted in Figure 15 show the importance of momentum convection in determining the flow pattern. The two cell flow pattern predicted by asymptotic analysis for a zone with heat supplied by a Gaussian source and for low Ma is only correct in that parameter region. Inertia causes the lower cell to compress the upper one against the melting feed rod giving the distorted patterns seen for higher Ma.

Publications and Presentations of Research Supported by Grant NSG-7656 (Since 1984)

Publications

1. G.M. Harriott and R.A. Brown, "Flow in a differentially rotated cylindrical drop at moderate Reynolds number," *J. Fluid Mech.* 144 (1984): 403-418.

2. L.H. Ungar and R.A. Brown, "Cellular interface morphologies in directional solidification. 2. The effect of grain boundaries," *Phys. Rev.* B 30 (1984): 3993-3999.

3. G.M. Harriott and R.A. Brown, "Flow structure and radial dopant segregation in small-scale floating zones," *J. Crystal Growth* 69 (1984): 589-604.

4. R.A. Brown, L.H. Ungar, and P.A.Adornato, "Convection, Segregation and interface morphology in directional solidification," *Proceedings of the Aachen Workshop on Solidification and Microgravity*, ed. P. Sahm (Aachen, West Germany, 1984), pp. 127-157.

5. R.A. Brown, "Status of modeling of convection, segregation, and interface morphology in melt growth of semiconductor materials," *Proceedings of Workshop on Microgravity Science and Applications* (National Research Council, December 1984).

6. E.D. Bourret, J.J. Derby and R.A. Brown, "One-dimensional modelling of transients in directional solidification of nondilute binary alloys," *J. Crystal Growth* 71 (1985): 587-596.

7. L.H. Ungar, M.B. Bennett, and R.A. Brown,, "Cellular interface morphologies in directional solidification. 3. The effect of coupled heat transfer," *Phys. Rev.* B 31 (1985): 5923-5930.

8. L.H. Ungar and R.A. Brown, "Cellular interface morphologies in directional solidification. 4. The formation of deep cells," *Phys. Rev.* B 31(1985): 5931-5940

9. R.A. Brown, "Physical process modelling: large-scale integration for complex physical system," *Proceedings of the NSF Workshop on Large-Scale Scientific Computing in the Chemical Process Industries* (December 1985).

10. R.A. Brown, "Convection and species transport," *Materials Sciences in Space*, eds. B. Feuerbacher, H. Hamacher, and R.J. Naumann (Berlin:Springer-Verlag, 1986), pp. 55-94.

11. R.A. Brown, "Modelling of transport processes in melt crystal growth," *Proceedings of the First International Conference on the Processing of Electronic Materials*, ed. C. Law (New York:Springer-Verlag, 1986, in press).

12. J.L. Duranceau and R.A. Brown, " A thermal-capillary model for the floating zone crystal growth process," *J. Crystal Growth* 75 (1986): 367-389.

13. P.M. Adornato and R.A. Brown, "The effect of ampoule on convection and segregation during vertical Bridgman growth of dilute and nondilute binary alloys," *J. Crystal Growth* 80 (1987): 155-190.

14. P.M. Adornato and R.A. Brown, "Petrov-Galerkin methods for natural convection in directional solidification of binary alloys," *Int'l. J. Numer. Meths Fluids* 7 (1987): xxx-xxx.

15. P. Sackinger, R.A. Brown, and G.B. McFadden, "Eigenfunction expansions for determining structure of natural convection in a vertical cylinder heated from below," J. Fluid Mech. (1987, submitted).

16. L.H. Ungar, N. Ramprasad, and R.A. Brown, "Finite element methods for unsteady solidification problems arising in the prediction of morphological structure," *J. Sci. Comput.* (1987, submitted).

17. D.-H. Kim, P.M. Adornato, and R.A. Brown, "Effect of vertical magnetic field on convection and segregation in vertical Bridgman crystal growth," *J. Crystal Growth* (1987, submitted).

18. F.T. Geyling, M.J. Crochet, and R.A. Brown, "Computer simulation of bulk crystal growth; a link between basic research and product engineering," *Science* (1987, in preparation).

19. N. Ramprasad, M.J. Bennett, and R.A. Brown, "Wavelength dependence of cellular forms for directional solidification cells with finite depth," *Physical Review B* (1987, submitted).

20. R.A.Brown, "Transport processes in melt crystal growth," *Chemical Engineering in Microelectronics*, ACS Volume, eds. K.F. Jensen and D. Hess (1987, in press).

21. R.A. Brown, "Convection and solidification in melt crystal growth," *Advanced Crystal Growth*, ed. P. Dryburgh (1987, in press).

22. L.G. Leal and R.A. Brown, "Fluid Mechanics of Microstructure Fluids," Report to NSF on Fluid Mechanics (1987, in press).

23. R.A. Brown, "Numerical analysis of solidification microstructure," *Supercomputer Research in Chemistry and Chemical Engineering*, ed. D.G. Truhlar and K.F. Jensen, ACS Symposium Series (1987, in press).

24. R.A. Brown, L.J. Atherton, J.J. Derby, P.A. Sackinger, and P.D. Thomas, "Modelling of Czochralski crystal growth," *Proceedings of the Fifth Inter. Conf. on Numerical Methods in Thermal Problem*, (1987, in preparation).

25. M.J. Bennett, R.A. Brown, and L.H. Ungar, "Nonlinear Interactions of Interface Structures of Differing Wavelength in Directional Solidification," *Proceedings of the 1986 Inter. Symposium on the Physics of Structure Formation* (1987, in press).

Presentations (Since November 1985)

26. R.A. Brown, "Large-Scale Numerical Calculation Applied to Melt Crystal Growth," Department of Chemical Engineering, University of Michigan, Ann Arbor, December 1985.

27. R.A. Brown, "Nonlinear Analysis of Microscopic Pattern Formation in Directional Solidification," Department of Computer Science, Yale University, New Haven, February 1986.

28. R.A. Brown, "Large-Scale Computer Simulation of Microscopic Transport Phenomena in Materials Processing," Department of Chemical Engineering, University of California at Berkeley, Berkeley Lecture, Berkeley, March 1986.

29. R.A. Brown, "Models of Melt Crystal Growth," Department of Chemical Engineering, University of California at Berkeley, Berkeley, March 1986.

30. R.A. Brown, "Nonlinear Analysis of Transport Processes," Six Lecture Series, Department of Chemical Engineering and the Applied Mathematics Program, Princeton University, May 1986.

31. R.A. Brown, "Microscopic Pattern Formation in Directional Solidification," Department of Chemical Engineering, Cornell University, Ithaca, October 1986.

32. M.J. Bennett, R.A. Brown, and L.H. Ungar, "Transitions in Microscopic Melt/Solid Interface Morphologies During Directional Solidification," Invited paper at the SIAM Fall Meeting, Tempe, October 1985.

33. R.A. Brown and P.M. Adornato, "Convection, Segregation and Interface Morphology during Directional Solidification," AIChE Annual Meeting, Chicago, November 1985.

34. P.A. Sackinger and R.A. Brown, "Nonlinear Transitions in Natural Convection Inside a Cylinder Heated from Below," AIChE Annual Meeting, Chicago, November 1985.

35. R.A.Brown, M.J. Bennett, and L.H. Ungar, "Nonlinear Dynamics of Two-Dimensional Cellular Solidification," Invited paper at the Engineering Foundation Workshop on Partially Solidified Systems, Fallen Leaf Lake, May 1986.

36. R.A. Brown, "Overview of Process Modelling," Plenary lecture at the National Forum on the Forum on the Future of Automated Materials Processing in the United States, National Bureau of Standards, May 1986.

37. R.A. Brown and M.J. Bennett, "Chaotic Interaction of Shallow Cells During Directional Solidification," Tenth U.S. Congress of Applied Mechanics, Austin, June 1986.

38. D.-Y. Kim, P.M. Adornato, and R.A. Brown, "Prediction of Dopant Segregation and Melt/Solid Interface Shape for Vertical Bridgman Growth with a Vertical Magnetic Field," VII International Conference on Crystal Growth, York, July 1986.

39. M.J. Bennett and R.A. Brown, "Chaotic Interactions of Shallow Cells During Directional Solidification," VII International Conference on Crystal Growth, York, July 1986.

40. R.A. Brown, "Modelling of Convection and Mass Transport in Melt Crystal Growth," Invited Lecture at the 6th International Summer School on Crystal Growth," Edinburgh, July 1986.

41. R.A. Brown, "Transport Processes in Directional Solidification on Earth and in Microgravity," Invited Lecture at the 33rd Annual Meeting of American Astronautical Society, Boulder, October 1986.

Personnel

Dr. P.M. Adornato, Ph.D. from MIT, January 1986, With Mobil Research and Development Laboratory, Paulsboro, NJ.

Mr. J.L. Duranceau, in sixth year of study toward Ph.D. Primary developer of finite element analysis for floating zone system. Supported by NASA.

Mr. P. Sackinger, in fifth year of study toward Ph.D. Research into nonlinear transitions in buoyancy-driven convection. Partially supported by NASA.

Mr. M.J. Bennett, in fifth year of study toward Ph.D. Research into nonlinear dynamics of cellular solidification. Partially supported by NASA.

Mr. D.H. Kim, in third year of study toward Ph.D. Research into convection and segregation in vertical Bridgman growth. Partially supported by NASA.

Mr. John Lee, in second year of study toward Ph.D. Developer of experimental system for study of dynamics of solidification for two-dimensional cells. Primarily supported by NASA.

N89-13677 56-29

175209

13P

Heat Flow Control and Segregation in Directional Solidification: Development of an Experimental and Theoretical Basis for Bridgman-Type Growth Experiments in a Microgravity Environment

Principal Investigator: Professor A.F. Witt

MJ 700808

Abstract

Within the framework of the proposed research, emphasis was placed on application of magnetic fields to semiconductor growth systems. Through complementary support by the Air Force and DARPA, we were able to acquire a superconducting magnet which can provide axial magnetic fields of up to 30 kGauss for melt stabilization in the NASA facility for heat pipe based vertical Bridgman-Stockbarger growth. It was found that axial fields up to 3 kGauss do not affect the growth behavior nor the macro-segregation behavior in the system Ge(Ga). Applied fields are found to significantly alter the radial dopant distribution, which is attributed to alterations in the spatial orientation of convective cells. Increasing the applied magnet field to 30 kGauss is found to have a fundamental effect on dopant segregation. The initial transient segregation behavior is identical with that predicted by Tiller et al. for diffusion controlled plane front solidification. Within the transient region, the dopant concentration increased by in excess of 600%, a concentration increase which in the magnitude has thus far only been observed in the ASTP experiment conducted in the reduced gravity environment of space. While the apparent achievement of diffusion controlled growth, as indicated by theory, is contingent on the validity of the available database, the experimental results demonstrate that magnetic melt stabilization can be valuable in emulating a limited spectrum of reduced gravity conditions. The experiments also point to the need, in space, for extended equilibration of melts prior to solidification, and alternatively, at the need for force convective mixing in a microgravity environment.

Emphasis was also place on the exploration of the potential of KC-135 flights for preliminary studies of the effects of reduced gravity environment on the wetting behavior of semiconductor systems in growth configuration. The experiments indicated different solidification characteristics; however, it was not possible to obtain quantitative data on wetting. The primary problem consisted of deficiencies of the available hardware. The limited number of experiments conducted does not permit any conclusions on the merits of KC-135 flights for semiconductor processing research. It is established, however, that the effective use of this facility will require acquisition of appropriate hardware.

At professional meetings, presentations were made on the potential of reduced gravity environment of R&D in materials processing.

Dopant Segregation During Vertical Bridgman-Stockbarger Growth with Melt Stabilization by Strong Axial Magnetic Fields

The effects of axial magnetic fields on dopant segregation during crystal growth in a seeded vertical Bridgman-Stockbarger configuration (Fig. 1) were investigated with gallium-doped germani-

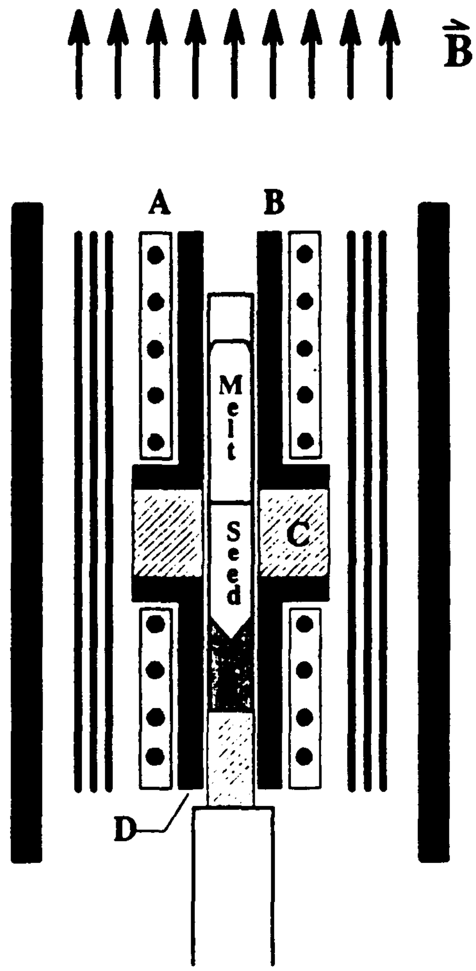

Figure 1. Schematic representation of vertical magnetic Bridgman-Stockbarger growth system: A. heaters, B. heat leveler, C. diabatic gradient control region, D. sodium heat pipe (inconel).

um. The growth system consisted of vertically aligned resistance heated high and low temperature zones which were separated by a 6 cm long diabatic gradient control region;[1] this system provided quantifiable and controllable thermal boundary conditions for the growth cavity (20 mm diameter). For melt stabilization, a superconducting magnet capable of generating vertical magnetic fields of up to 30 kGauss was installed coaxially about the growth system. The charges, polycrystalline ingots and seeds of [100] orientation, were contained in quartz ampoules of 15 mm ID (17 mm OD).

The growth procedure was as follows: the ampoules were inserted to a predetermined position within the growth cavity and the system was purged with argon and maintained at a dynamic over-pressure of about 10 torr; after activating the magnet, power was set at 980 and 750°C, respectively achieving seed meltback of about 1 cm with the growth interface being located at 0.5 cm below the heat leveler. Following equilibration of 30 min, growth was initiated by lowering the charge at a constant rate (10μm/s in the reported experiments). After the charge was solidified, the magnetic field was ramped down and the heater power was reduced to zero over a period of 10 hrs. The grown single crystals were removed, appropriately cut, polished, and subjected to differential chemical etching.[2] Macro-segregation profiles were determined through spreading resistance measurements (ASR-100) on longitudinal crystal segments which contained on their surface the geometric crystal axis. The crystal slices, mounted with In-Sn solder on brass disks, were measured in single point mode at spacings of 10 and 100 μm for micro and macro-segregation analyses respectively. The reported data (Fig. 2) are based on average values of three parallel axial scans (center; left and right

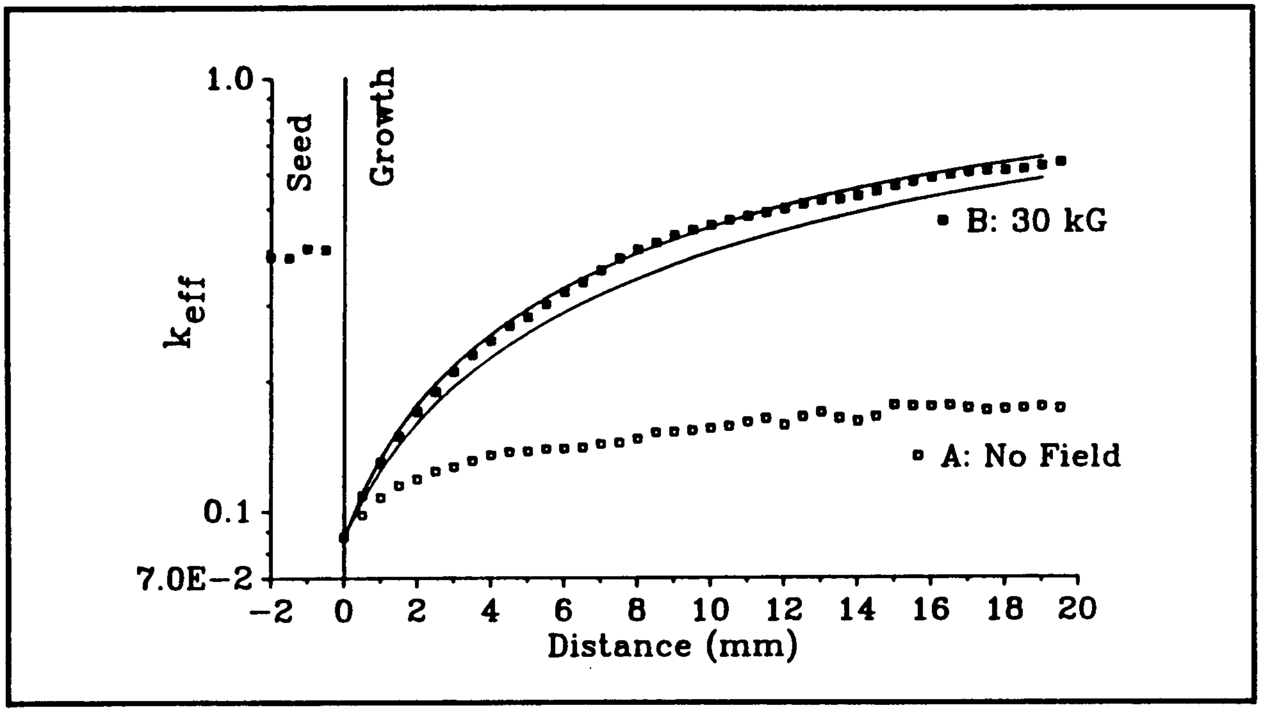

Figure 2. Macrosegregation analysis for growth of Ga-doped germanium. (a) Segregation for growth in the absence of a magnetic field; (b) segregation with an applied axial magnetic field of 30 kGauss. the solid curves about the data for growth at 30 kGauss correspond to theoretical predictions of segregation according to Tiller[4] using D values of 1.7 (upper curve) and 2.1 x 10^{-4} cm^2/s (lower curve.

periphery, 2 mm form the crystal edge) at common longitudinal positions. To ascertain the degree of radial uniformity of dopant distribution, assumed in the macrosegregation analyses, a limited number of radial scans were made on the longitudinal slices. Analyses of multiple radial scans on wafers (from other crystals grown in this system) confirmed radial symmetry of dopant distribution.

Differential etching analyses on all crystals grown in this system revealed rotational and non-rotational dopant striations in the (Czochralski grown) seed portion and the original melt-crystal interface; no striations were observed in any of the crystal portions grown in the Bridgman-Stockbarger system. The curvature of the growth interface in the crystal grown with high magnetic field stabilization (30 kGauss) resulted in a concave (into the solid) morphology with a maximum central deviation from planarity of 20 μm. This interface deflection is almost an order of magnitude less than that observed without stabilization in this thermal configuration.[1]

Figure 2 shows axial composition profiles for the initial 2 cm of crystal growth; curve A was obtained for growth without magnetic field stabilization and curve B for growth with melt stabilization by high axial magnetic field (30 kGauss). In this figure the dopant concentrations, C_s are normalized with $k_0/C_s(0)$ to permit a convenient comparative analysis [$k_0 = 0.087$, the equilibrium distribution coefficient for Ga in Ge, and $C_s(0)$ is the Ga concentration in the crystal portion that was first solidified ($x = 0$)]. Normalization thus yields the effective distribution coefficient [$k_{eff} = C_s \cdot k_0/C_s(0)$] for conditions under which the bulk melt concentration remains constant during solidification. Curve A in Fig. 2 indicates that during conventional , nonstabilized solidification at a rate of 10 μm/s the dopant concentration in the growing crystal increases by a factor of 2 during the first 2.0 cm of growth. The major fraction of the concentration increase occurs within approximately 1 mm of the initial growth interface which reflects the initial build-up of a solute boundary layer. The subsequent segregation behavior is indicative of <u>pronounced</u> thermal convection effects (driven by unavoidable radial thermal gradients in the melt). Thus the observed gradual increase in dopant concentration does not reflect a further increase in the thickness of the solute boundary layer; i.e., it does not reflect an increase in k_{eff}. In the present context it is important to note that the average longitudinal composition profiles obtained for growth without magnetic melt stabilization are virtually indistinguishable from those obtained during growth with melt stabilization by axial and transverse magnetic fields of up to 3 kGauss.[3] Melt stabilization by low fields did not reveal any decrease in macrosegregation. However, it revealed significant changes in radial segregation[3] considered indicative of pronounced magnetic field induced alterations in the patterns of convective melt flows. This phenomenon is currently the subject of further investigations.

Curve B is the normalized initial axial macrosegregation profile for a germanium crystal grown at a rate of 10μm/s in the presence of an axial magnetic field of 30 kGauss. It is observed that the radially averaged dopant concentration under these conditions increased over the first 20 mm of growth by more than a factor of 6 which strongly suggests that the melt stabilization by high magnetic fields led to a reduction or absence of convective interference with segregation. The effectiveness of the magnetic melt stabilization can be assessed through computation of the "approximate critical transient growth distance" (x_{cr}) according to the theory of diffusion controlled plane front solidification by Tiller et al. (4). This theory predicts for diffusion controlled growth the axial dopant concentration, C_s, with growth distance (x):

$$C_S(x) = C_0[1 - k_0)e^{-k_0 Rx/D}] \tag{1}$$

where C_0 is the initial dopant concentration in the melt given by $C_s(0)/k_0$, D is the diffusion coefficient of Ga in the Ge melt (2.1×10^{-4} cm^2/s), and R is the growth rate (10 μm/s). Assuming applicability of eq. [1] to solidification of the magnetically stabilized Ga doped Ge melt, the dopant concentration (Cs) in the crystal is expected to have increased from $C_0 \cdot k_0$ to $C_0 \cdot (1-1/e) = C_0 \times 0.63$ after a critical growth length, x_{cr}, given by $D/(k_0R)$. (This approximation is justifiable since k_o is $<< 1$.) Using a recent publication by Bourret et al. as database,[5] x_{cr}, the critial growth distance, is computed to be 2.4 cm. The experimental segregation data, on the other hand, indicate (Fig. 2) that $C_s = C_0 \times 0.63$ is achieved at $x_{cr} = 1.9$ cm, less than theoretically predicted for diffusion controlled segregation. Since any convective interference with segregation will increase rather than decrease the critical length (xcr), the experimental data appear to conform with diffusion controlled segregation; the discrepancy between theory and experiment is taken to reflect limitations of the database. For the readers' convenience, graphic presentations of eq. [1] are superimposed on the experimental data in Fig. 2. (The two curves correspond to D values of 1.7 and 2.1×10^{-4} cm^2/s.)

The presently reported preliminary results on the effects of melt stabilization by high axial magnetic fields were obtained within the framework of ongoing research on heat and mass transport control directional solidification. Assuming applicability of the theory of plane front solidification and validity of the database, the results of the transient segregation analysis suggest that diffusion controlled solidification has been achieved in vertical Bridgman-Stockbarger growth through melt stabilization by an axial magnetic field of 30 kGauss. This finding appears to confirm theoretical predictions by Oreper et al.,[6] Kim et al.,[7] and Motakef.[8] A detailed study of segregation beyond the initial transient is currently in progress.

Electronic Materials Processing and The Microgravity Environment

Introduction

Progress in solid state technology during the past two decades was dominated by innovative device design and engineering. Projected further advances, according to steadily mounting evidence, are contingent on the availability of electronic materials with a degree of crystalline and chemical perfection which exceeds significantly the capabilities of established processing technology. When considering the background and nature of the existing technological deficiencies, the exploration of the potential of reduced gravity environment of electronic materials processing and for related R&D appears not only attractive, but also logical. Manufacturing technology centers undergo global redistribution and trends indicate clearly that developing countries assume at a steadily increasing rate a primary supplier position in the advanced materials sector. While this shift in manufacturing activities is proceeding, the related R&D activities are almost exclusively conducted in the traditional centers of high technology. By definition, the developing countries become developed countries and are as such expected to also provide for timely advances of their adopted technologies. The broad-based involvement of developing countries in the exploration and anticipated exploitation of microgravity environment for electronic materials processing must thus not only be considered as desirable, but rather as mandatory.

Status

The fundamental semiconductor property requirements dictated by device technology are matrices with controllable, uniformly distributed charge carriers of maximized mobility and lifetime. This requirement translates into the need for semiconductor single crystals of uniform composition and a maximized degree of crystalline perfection. The complexity and changing nature of property requirements, dictated by device engineering, is reflected in some of the emerging GaAs device technology where a primary property requirement extends to the controlled introduction of uniformly distributed interactive point type defects.

Semiconductors of primary industrial concern, Si and Ge originally, now include in addition GaAs, GaP, InP, CdTe, and related ternary and quarternary compounds. All of these materials in bulk form are used either directly or indirectly (as substrates) for device fabrication.

The fundamental electrical properties are conventionally achieved through the incorporation of appropriate electrically active dopant elements into the single crystal semiconductor matrix while simultaneously keeping any contamination by impurities at an absolute minimum.

In excess of 90% of the semiconductor crystals used for device fabrication are produced by the Czochralski process: A single crystal seed of a particular orientation attached to a pulling rod is contacted with the semiconductor melt which is maintained in an inert atmosphere at a temperature somewhat above its melting point. After thermal equilibration, the seed is pulled (at a rate ranging from 0.1 to about 5"/hr) under simultaneous seed and crucible rotation (Fig. 3). Through appropriate temperature adjustments of the melt, the diameter of the growing crystal (ranging in weight from 3 to in excess of 50 kg) can be increased or decreased as desired. Inherent to this crystal growth configuration is radial heat input to the melt and the withdrawal of the crystal along the rotational axis of the system. Accordingly, the melt experiences radial and vertical thermal field distribution thus gives rise to convective melt flows which affect the growth behavior[9-12] as well as the incorporation of the dopant elements (Fig. 4). The driving force for convection in commercial-scale systems is of a magnitude which renders the resulting melt flows turbulent; they are characterized by significant time dependent velocity as well as temperature fluctuations.

These gravity induced melt flows affect the heat and mass transport in the bulk melt, control the nature of all associated boundary layers, and thus by-and-large dictate the crystalline and chemical

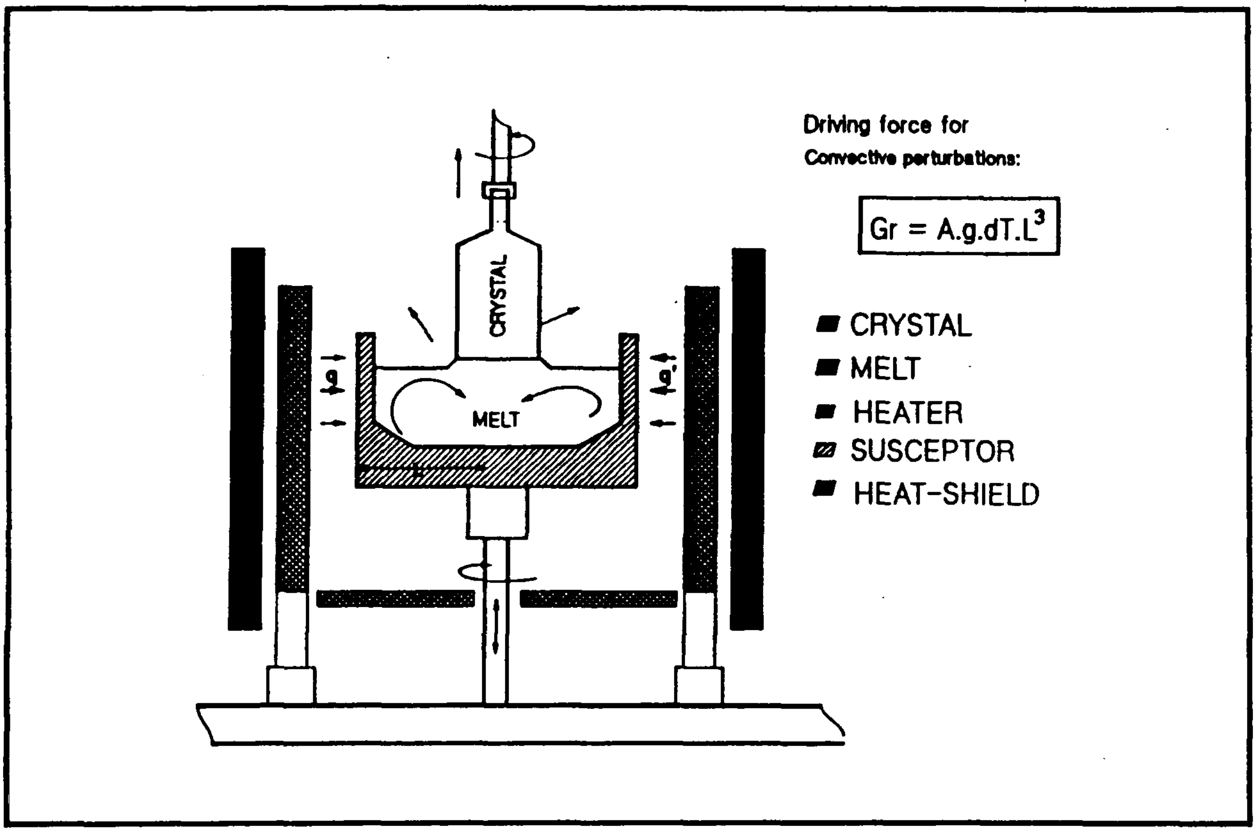

Figure 3. Conventional Czochralski configuration used for pulling of semiconductor single crystals from the melt. Notice the lateral, asymmetric heat input (q) giving rise to three-dimensional turbulent convective melt flows which adversely affect the crystal properties.

perfection of the forming crystal. Effects of concern that can be directly related to convection are summarized in Fig. 5. It should be noted also that inherent to processing on earth is the need for charge confinement and related to it, the potential of melt contamination. Gravity induced melt flows accelerate mass transport and for that reason are also responsible for increased impurity levels in crystals grown from or in containers. Containers, moreover, modify the thermal field distribution in growth systems and adversely affect heat transport control, a critical element in efforts to optimize crystal properties for particular device applications.

Semiconductors for advanced device applications, produced by the established growth technology, fail at a steadily increasing rate to meet property requirements and it si acknowledged that property requirements for projected device technology will likely not be met by presently practiced procedures.

Research aimed at the development of novel approaches to semiconductor growth are severely impeded by the fact that the theoretical framework for solidification and segregation is not quantitatively applicable to crystal growth systems, primarily because of convective interference and the existence of nonquantifiable boundary conditions.

Gravitational effects are clearly recognized as the primary cause of our inability to bridge the existing gap between theory and practice of crystal growth and are therefore the direct cause for our failure to achieve theoretical property limits in materials, the prerequisite for optimization of device performance. They are thus also responsible for industry's heavy reliance on proprietary empiricism in processing technology.

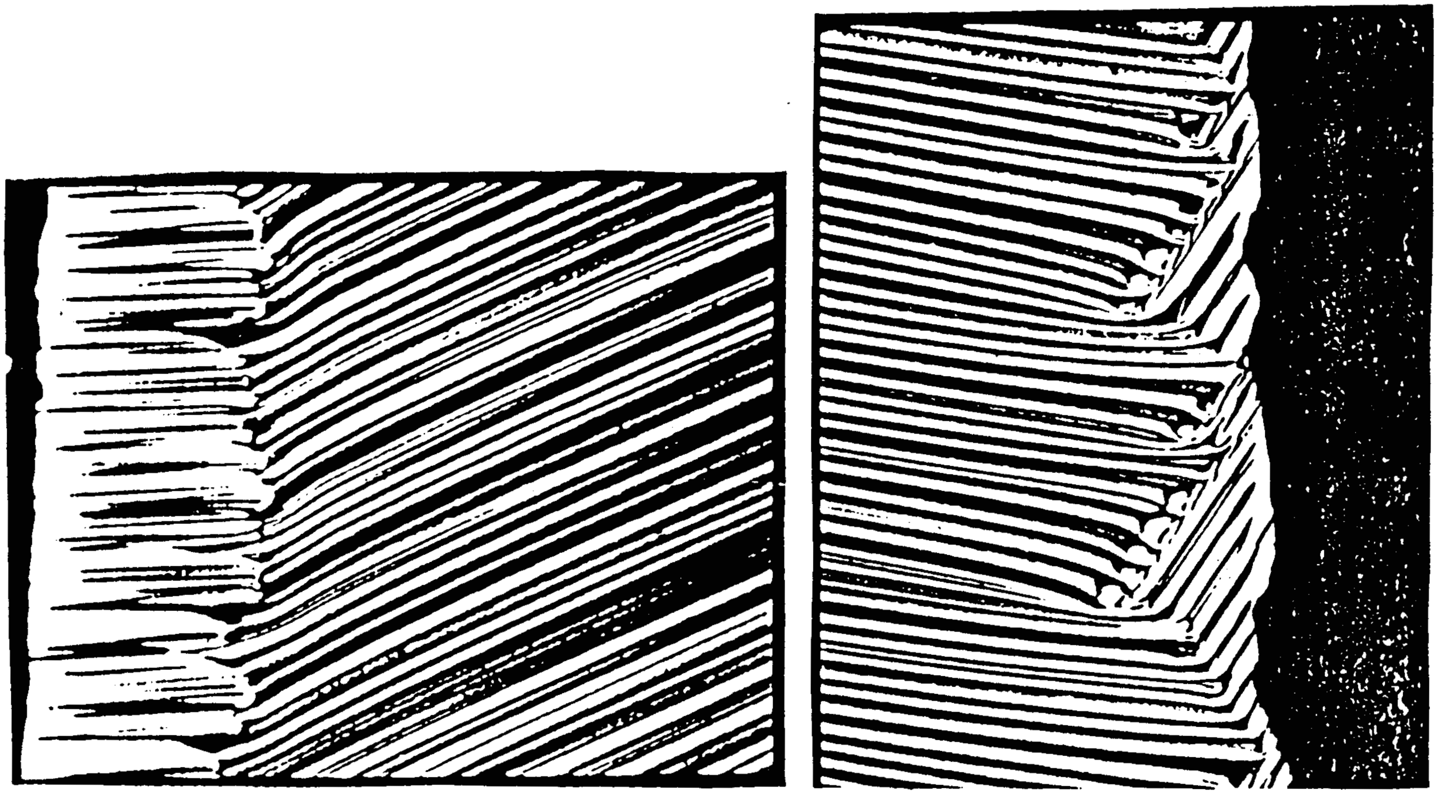

Figure 4. Interface contrast micrography (X600) of etched longitudinal section of doped silicon. The distinct intensity patterns reflect charge carrier fluctuations in the matrix caused by nonuniform dopant incorporation due to gravity induced convection.

Crystal Growth in a Reduced Gravity Environment

The driving force for convective melt flows in semiconductor growth systems is primarily controlled by the magnitude of the gravitational constant. Accordingly, thermal convection can be expected to be virtually absent in a microgravity environment where the g value is reduced by four to five orders of magnitude. This effect provided the primary motivation for the first semiconductor growth experiments in space.[13,14] These early space activities, conducted in relatively unsophisticated hardware, provided more question marks than answers to existing issues (Fig. 6). Most of all they exposed serious deficiencies in the database of these materials and processes. They also demonstrated that attempts to apply theory to growth experiments are severely limited by the nonquantifiable nature of prevailing boundary conditions.

Shortcomings in the design and execution of the space experiments notwithstanding, their impact on growth technology on earth and their stimulation of growth related R&D is conspicuous. A direct outgrowth of efforts aimed at emulating, to the extent possible, conditions prevailing in reduced gravity environment led to the evolution of magnetic melt stabilization and to the development of magnetic Czochralski growth as practiced in growth technology (Fig. 7). Heat transfer control, virtually neglected prior to these experiments, emerged as a primary issue and resulted in

Macrosegregation of dopants and impurities

Microsegregation of dopants and impurities

Deviations from stoichiometry

Formation and distribution of nonequilibrium point-defects

Formation of dislocations and other extended crystal-defects

Constitutional supercooling effects

Growth interface morphology controlled by convective heat-transport

Deterioration of radial vertical thermal gradients in the melt

Figure 5. Summary of the most conspicuous property deficiencies in melt-grown semiconductors that can be attributed to gravity-induced convective melt flows prevailing during their formation.

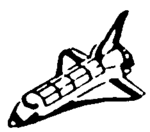

RESULTS:

- Diffusion controlled growth and segregation: ?
- Theory of thermo-capillarity: ?
- Theory of radial segregation: ?
- Wetting behaviour of the melt: ?
- Dopant effects on wetting behaviour: ?

Impact on technology:

- magnetic melt stabilization (MCZ)
- heat transport control by heatpipes
- development of confinement materials
- focus on modified Bridgman growth
- electro-epitaxy

Impact on R/D and science:

- Interface demarcation
- Magneto hydro-dynamics
- Thermo-capillarity
- Expert systems in growth control

Figure 6. Summary of results obtained from semiconductor growth experiments conducted in space and their impact on technology development.

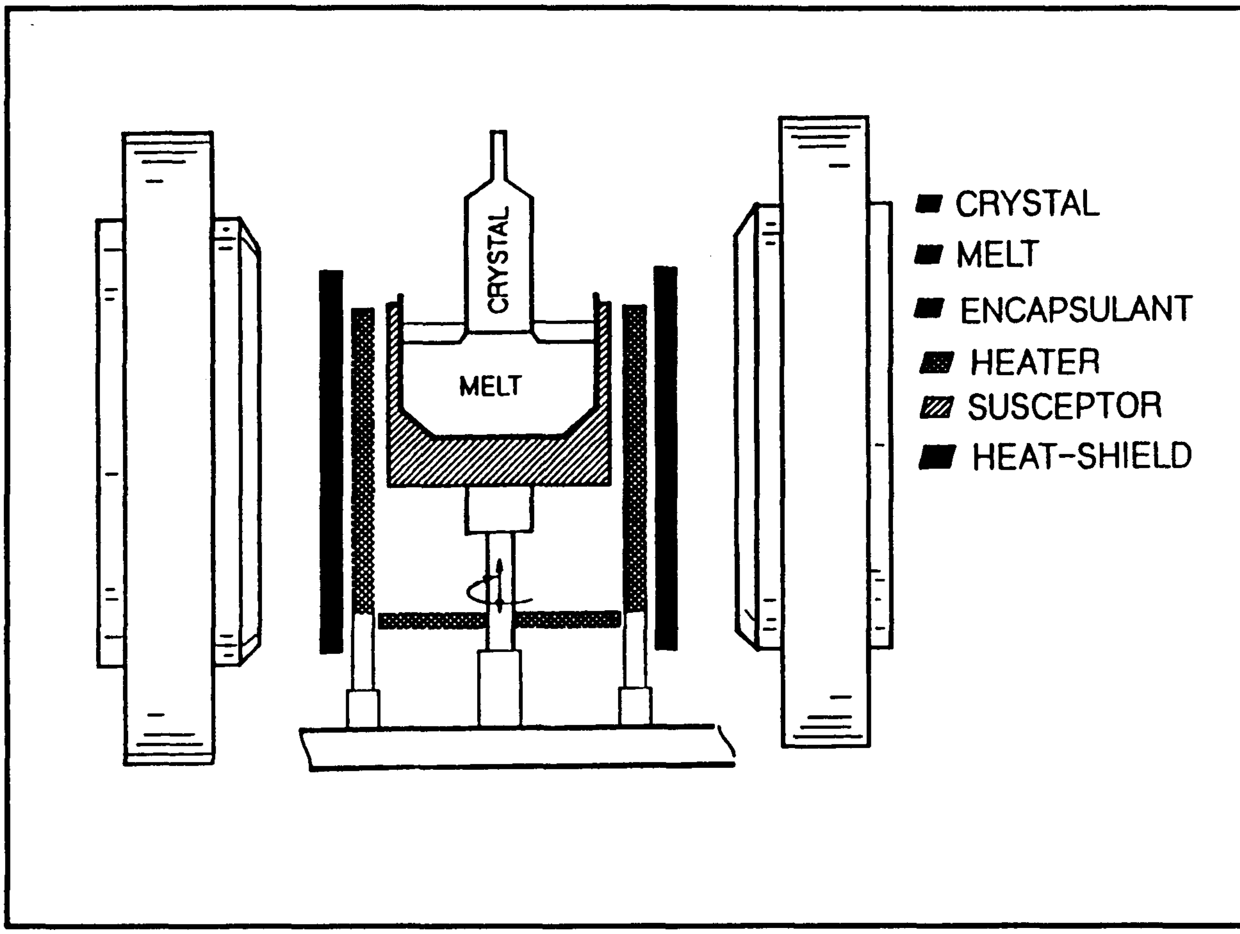

Figure 7. Modified Czochralski configuration for advanced semiconducotr growth. The modifications (magnetic melt stabilization, coaxial heat pipe between heater and crucible) constitute significant advances, which are based on results from experiments conducted in reduced gravity environments.

major efforts aimed at the development of high temperature heat pipes, now considered essential for the establishment of quantifiable boundary conditions are realized as the fundamental prerequisites for meaningful mathematical modeling activities of growth processes and ultimately for efforts aimed at model-based growth control schemes.

Outlook

Experiments in reduced gravity environment have focused attention on Bridgman type growth geometries, primarily because of the fundamental incompatibility of the conventional Czochralski geometry with space environment. These studies stimulated the application of heat pipes for heat transport control (Fig. 8) and resulted in the first applied modeling approach in which the theoretically predicted thermal field distribution was quantitatively confirmed by the experiment.[15,16] More recently this growth geometry (in gradient freeze configuration) has been shown to permit single crystal growth of InP and GaAs with unprecedented low dislocation density.[17] Of interest in context is the finding that vertical Bridgman growth, although characterized by stable axial thermal gradients, does exhibit pronounced thermally driven convective melt flows because of unavoidable radial temperature gradients. These convective melt flows which, as in Czochralski growth, adversely influence the growth and segregation behavior, remain virtually unaffected by axial or transverse magnetic fields of up to 0.3 T (Fig. 9). Increasing the strength of the applied magnetic field by one order of magnitude to 3 T, it is most recently found that convective melt flows in doped germanium are reduced to a point where they no longer interfere with dopant incorporation (Fig. 10); the

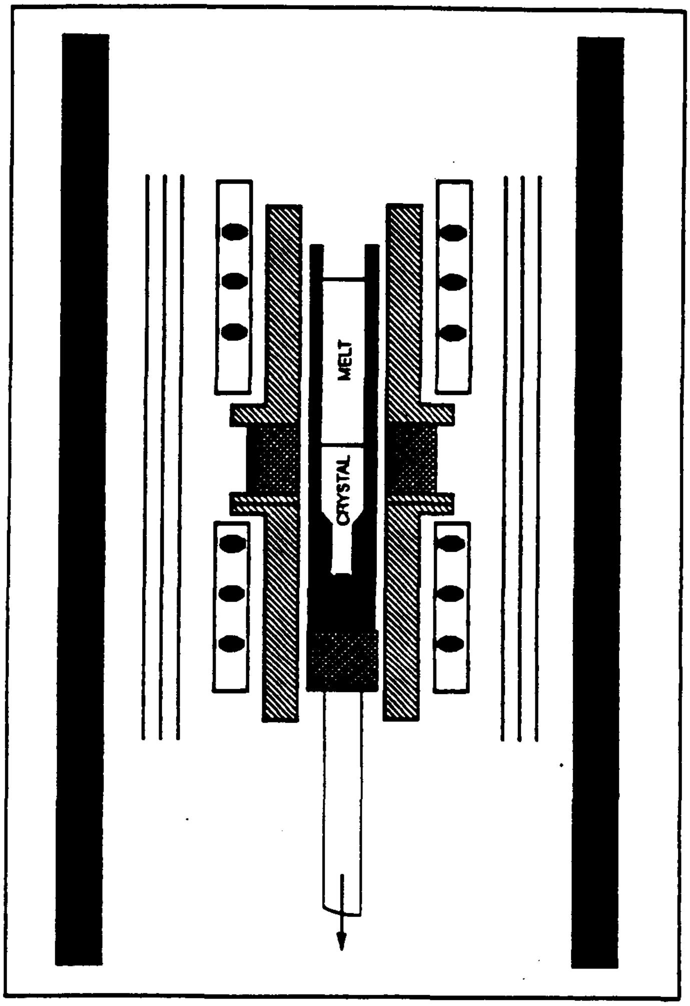

Figure 8. Modified vertical Bridgman-Stockbarger configuration for growth of semiconductor single crystals. This heat pipe based system provides for unprecedented heat transfer control and permits meaningful mathematical modeling.

segregation behavior exhibits characteristics which are very similar to those observed during crystal growth in a reduced gravity environment.

The results of growth experiments with magnetic melt stabilization are of technological interest, primarily because they indicate that convective flows in stabilized melts are laminar and the melt temperature is no longer subject to uncontrollable fluctuations. Such experiments, however, are still subject to other gravity induced side effects, such as melt contamination through interaction with the confinement materials and thermal field distortion due to heat conduction along the crucible walls. Finally, it must be realized that melt stabilization through magnetic fields is only possible in highly conductive melts which severely limits the range of its applicability.

Melt stabilization of growth systems by magnetic fields, in spite of shortcomings, clearly demonstrates elements of the potential of reduced gravity environment for electronic materials processing. The results suggest that growth of crystals (in space) with compositional homogeneity on both a micro- and macro-scale appears achievable. Also achievable appears to be the suppression of constitutional supercooling effects and heat transport control to a point where thermal stresses can be

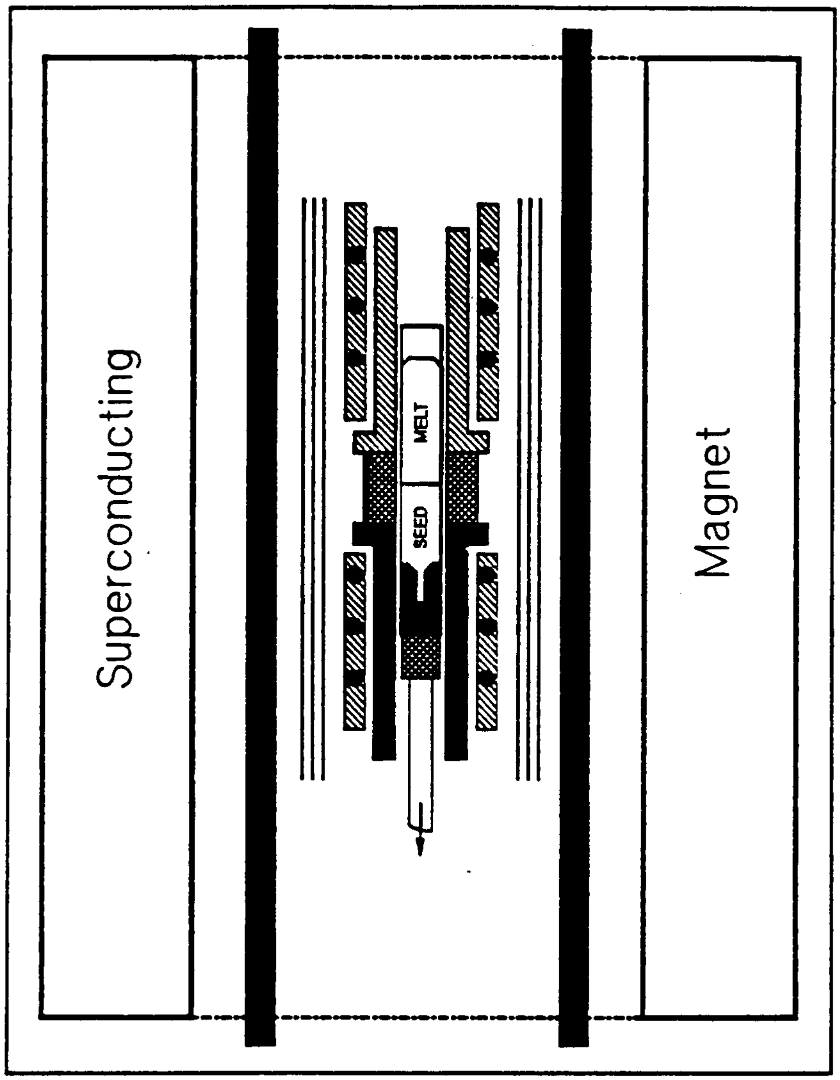

Figure 9. Vertical magnetic Bridgman configuration for growth of semiconducotr crystals with diffusion controlled dopant segregation. (Using a 3 T axial field, it has thus been possible to achieve a k_{eff} of 1 of segregation of Ga in Ge.)

maintained at levels of less than the critical resolved shear stress. The experiments as well as the underlying theory indicate unambiguously that realization of the full potential of space environment is contingent on the achievement of a high degree of heat transfer control, the establishment of quantifiable boundary conditions, and on the availability of a viable theoretical framework for solidification.

Considering the advances of processing technology on earth which resulted from the rather limited number space experiments, it is apparent that direct science and technology transfer from space experiments is an important element. Equally important for significant improvements of ground based operations is the broadening of the database which is expected to accompany experimentation in space.

The fundamental drawbacks of space experimentation relate to costs, limitations in access to space, and uncertainties in man-experiment interaction. Although costs for experiments in space will always be high, the costs for exploring the potential of reduced gravity environment, an element of

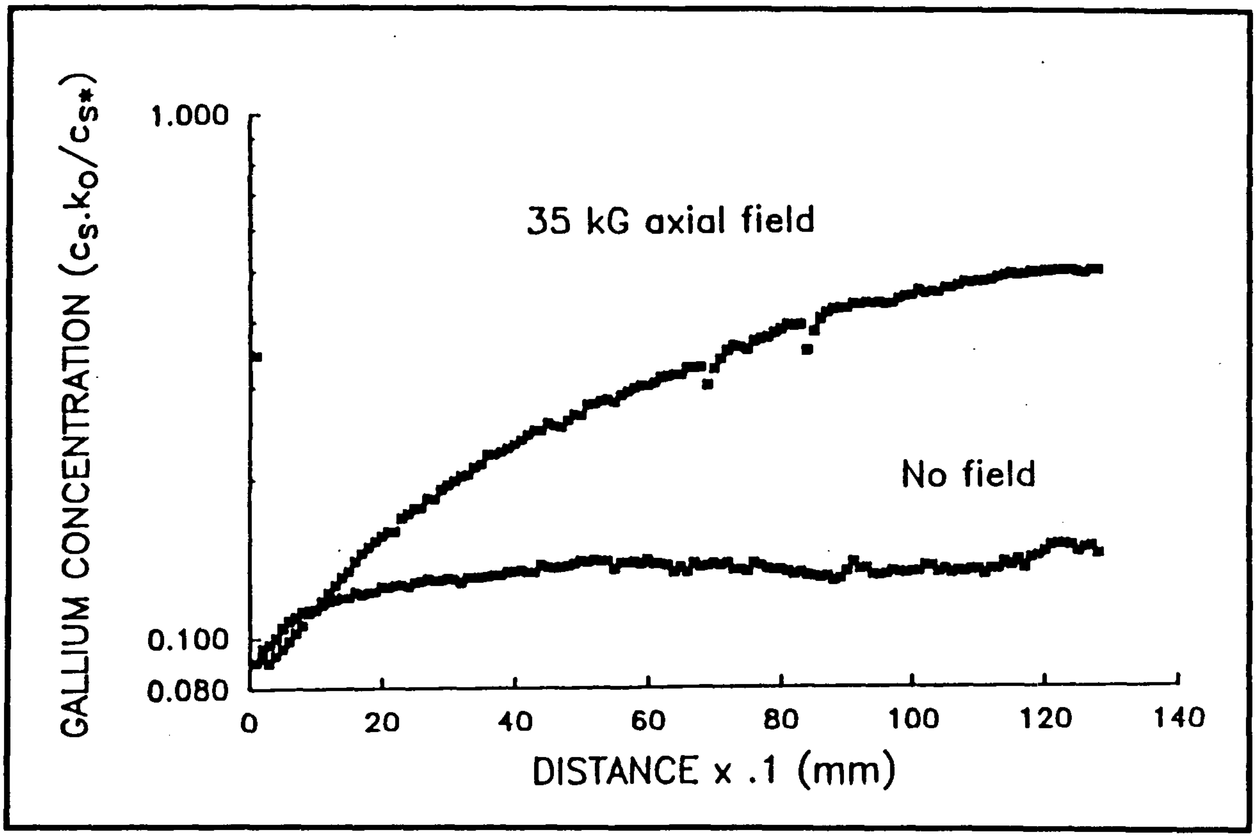

Figure 10. Macrosegregation behavior (of Ga in Ge) in a heat pipe based vertical Bridgman system with and without magnetic field stabilization. The transient segregation in the presence of the magnetic field indicates the absence of convective interference with dopant accumulation at the growth interface.

concern for developing nations, will become less as the scientific framework for processing activities is complemented by results obtained in space. A further cost reduction can be expected from process automation which will make it possible to reduce man-tended experiments to a minimum and allow experiment monitoring and control from the ground.

Conclusions

The capabilities of established semiconductor growth technology are considered inadequate to meet property requirements for projected advances of device technology. Encountered materials deficiencies, inadequate crystalline and chemical perfection, can primarily be related to gravitational interference with the melt growth process. It has been shown that semiconductors grown in a reduced gravity environment do not exhibit these deficiencies and that results of growth experiments in space can provide substantive input to the advancement of processing technology on earth.

Considering the fact that semiconductor manufacturing technology is at a steadily increasing rate being relocated to developing nations, their participation in the exploration and possible exploitation of the potential of space environment for semiconductor growth appears not only desirable but mandatory.

Reference List

1. C.A. Wang, "Analysis of Crystal Growth and Segregation in Vertical Bridgman Configuration," Ph.D. Thesis, Department of Materials Science and Engineering, Massachusetts Institute of Technology, Cambridge, MA (1984).

2. A.F. Witt, H.C. Gatos, M. Lichtensteiger, and C.J. Herman, "Crystal Growth and Segregation under Zero Gravity: Ge," *J. Electrochem. Soc.: Solid State Sci. and Tech.* 125 (11, 1978): 1832-1840.

3. D.H. Matthiesen, M.J. Wargo, and A.F. Witt, "Opportunities for Academic Research in Micro-Gravity Environment: Crystal Growth," *Opportunities for Academic Research in a Low-Gravity Environment*, eds. G.A. Hazelrigg and J.M. Reynolds, Vol. 108 of Prog. in Astro. and Aero. (New York:AIAA, 1986) pp. 125-144.

4. W.A. Tiller, K.A. Jackson, J.W. Rutter, and B. Chalmers, "The Redistribution of Solute Atoms During the Solidification of Metals," *Acta Metallurgica* 1 (July 1953): 428-437.

5. E.D. Bourret, J.J. Favier, and O. Bourrel, "Measurement of the Diffusion Coefficient of Gallium in Molten Germanium," *J. Electrochem. Soc.: Solid State Sci. and Tech.* 128 (11, 1981): 2437-2439.

6. G.M. Oreper and J. Szekely, "The Effect of a Magnetic Field on Transport Phenomena in a Bridgman-Stockbarger Crystal Growth," *J. Crystal Growth* 67 (1984): 405-419.

7. D.H. Kim, P.M. Adornato, and R.A. Brown, "Effect of Vertical Magnetic Field on Convection and Segregation in Vertical Bridgman Crystal Growth," *J. Crystal Growth* (1987, submitted for publication).

8. P.R. Griffin and S. Motakef, "Influence of Applied Magnetic Fields on Fluid Dynamics and Mass Transfer in Semiconductor Crystals Grown by the Bridgman-Stockbarger Technique," *J. Crystal Growth* (1987, in preparation).

9. K.E. Benson, "Radial Solute Distribution in Czochralski-Grown Silicon Crystals," *Electrochem. Tech.* 3 (11-12, 1965); 332-335.

10. A.F. Witt, M. Lichtensteiger, and H.C. Gatos, "Experimental Approach to the Quantitative Determination of Dopant Segregation During Crystal Growth on a Microscale: Ga-Doped Ge," *J. Electrochem. Soc.* 120 (8,1973); 1119-1123.

11. W. Keller and A. Muhlbauer, "Float-Zoned Silicon with Homogeneous Dopant Distribution," *Phys. Stat. Sol.* A25 (1974); 149-152.